NASA-CR-203100

009226

THE ENVIRONMENTAL IMPACT OF INTRA-CLUSTER MEDIUM ON THE INTERSTELLAR MEDIUM IN EARLY TYPE GALAXIES

NASA Grant NAG5-2049

Semiannual Reports

1 August 1993 – 31 January 1994, 1 February 1994 – 31 July 1994,
and 1 August 1994 – 31 January 1995

Annual Report

1 August 1995 – 31 July 1996

Principal Investigator
Dr. Ginevra Trinchieri

November 1993

Prepared for:

National Aeronautics and Space Administration
Goddard Space Flight Center
Greenbelt, Maryland 20771

Smithsonian Institution
Astrophysical Observatory
Cambridge, Massachusetts 02138

The Smithsonian Astrophysical Observatory
is a member of the
Harvard-Smithsonian Center for Astrophysics

The NASA Technical Officer for this grant is Dr. Robert Petre, Code 666, Laboratory for High Energy Astrophysics, Space Sciences Directorate, Goddard Space Flight Center, Greenbelt, MD 20771.

Your thesaurus codes are:
11()

ASTRONOMY AND ASTROPHYSICS
24.9.1996

G. Trinchieri[1,2] and L. Noris[3]

[1] Osservatorio Astronomico di Brera, Via Brera 28, 20121 Milano ITALY
[2] Max Planck Institut für extraterrestrische Physik, Gießenbachstraße, D-85740 Garching, Federal Republic of Germany
[3] Università degli Studi di Milano

DRAFT

Abstract. XXXXXXXX DRAFT XXXXXXX DRAFT XXXXXXXXX DRAFT XXXXXXXXXXXX

High resolution X-ray images of three early type galaxies observed with the ROSAT HRI are presented. Data for NGC 1553 and NGC 5846 indicate that the emission is highly irregular, with interesting features at different scales. The gas temperatures also vary both with the galactocentric radius an in correspondence to regions of higher emission and denser material.

Strikingly similar features are observed in the X-ray and Hα morphologies of NGC 1553 and NGC 5846, while smooth, regular isophotes are observed in NGC 4649 at both wavelengths. A connection between these two kinds of emission therefore seems likely.

Key words: - Galaxies: elliptical and lenticular - Galaxies: ISM - Galaxies: individual:

1. Introduction

The existence of a hot interstellar medium in bright early-type galaxies and some of its properties have been established in the past $\sim$ 15 years with data first from *Einstein* and more recently from ROSAT and ASCA. X-ray images have shown the presence of diffuse emission at least coextensive with the the stellar component in the x-ray bright early type galaxies. Average temperatures and radial temperature gradients have been measured. In general, temperatures of 0.5-1.5 keV are a common property of these galaxies, with cooling times typically much shorter than a Hubble time.

Coexisting with the hot ISM, a cooler ("warm") component has been mapped in Hα in several X-ray bright objects (Kim 1989; Trinchieri & Di Serego 1991; Shields 1991; Goudfrooij et al. 1994; Buson et al. 1994; Singh et al. 1995; diSerego et al in preparation). The morphology of this emission can be either relatively smooth and azimuthally symmetric or exhibit filamentary structures, arcs and/or rings. Although clearly extended, it is generally confined to the innermost regions of the galaxies, often within $\sim$ 1 kpc, and it is relatively faint and hard to detect properly. To date, the study of the relation between hotter and cooler gas has been restricted to a handful of galaxies. Moreover, only the statistical comparison of the total X-ray and Hα luminosities has been studied. Morphological comparisons require high-resolution X-ray data which is only recently becoming available with the ROSAT HRI observations. The comparison of the luminosities in optical emission lines and in X-rays suggests that while galaxies with a larger X-ray emitting gas component also show more powerful line emission than objects with a smaller hot interstellar medium, the scatter in the relation is significant, implying that other parameters play a role in the production of optical lines (see e.g., Trinchieri & Di Serego 1991).

There are however new high resolution data at both X-ray and optical wavelengths that suggest a very close connection between these two gas phases. As shown by the preliminary data presented by Trinchieri & Noris (1995), both gross and finer morphological similarities are found in the X-ray and Hα maps of NGC 1553 and NGC 5846. We present here a more comprehensive investigation of these similarities. Section 2 presents the X-ray data analysis of NGC 1553, NGC 4649 and NGC 5846 (?? NGC 1332 should be added). The Hα data obtained from the literature (Trinchieri & diSerego 1991, diSerego et al. 1996) are compared to the X-ray maps in Section 3, and a discussion of the results is presented in Section 4.

Send offprint requests to: G. Trinchieri

ROSAT HRI data of the sample galaxies have been obtained in several observing runs, as detailed in Table 1. A few standard procedures have been applied to the data, as briefly summarized below. To analyze the X-ray data we have used mainly the PROS software (Worral et al 1992) developed under the IRAF (Tody 1986) environment. For each field, a radial distribution of the detected emission is produced in concentric annuli centered at the X-ray peak and extending out to the edges of the field. The radial profiles (Fig. 1) indicate that outside of r=5′, 7′ and 7′ for NGC 1553, NGC 4649 and NGC5846 respectively, the emission is relatively constant with radius, as expected from an uniform illumination (such as due to isotropic sky emission and particle contamination) of the instrument field of view (The ROSAT Users' Handbook, David et al. 1995). We have therefore used the region outside of these radii to estimate the background. Even though a small vignetting effect is evident in the form of a radial gradient in the data (in particular after the selection on the raw energy channels, see later), the correction is small, and a local estimate allows us to better estimate the statistical uncertainties in the subtraction of the background. To minimize the vignetting effect we have selected the annulus at $8' - 10'$ radial distances for all objects, that should avoid emission from the source, while being relatively near the field's center.

The HRI has not been calibrated in energy, however the data retain the information about the Pulse Height Amplitude Channel (PHA, in the range 1 to 15, see The ROSAT Users' Handbook) in which each incoming photon was detected. Therefore, although we cannot retrieve the energy distribution of the photons, we can examine the PHA of the photons extracted from different regions to look for differences. This is particularly useful to enhance the significance of the detection. In fact the spectral distribution of the "source" and of the background are different, as shown in Fig 2. We have therefore used only those PHA channels in which the signal is significantly higher than the background, namely PHA 1 to 7 for NGC 1553 and NGC 4649, and PHA 1 to 9 for NGC 5846. The radial profiles corresponding to this selection is also plotted in Fig. 1.

Both NGC 4649 and NGC 5846 were observed in two occasions by the ROSAT HRI, as reported in Tab. 1. The first observation of NGC 4649 is of only $\sim$ 2000 sec., while the second observation is much longer ($\sim$ 12000 sec.), and will therefore dominate in the subsequent analysis. However, since the image obtained from the short exposure seemed to be consistent with the longer one, we have merged the two in order to increase the statistical significance. The two observations of NGC 5846 are of similar length, and therefore each will have approximately equal weight in the final merged image. We have therefore first analyzed each of the two images separately, to check for possible differences. With the exception of the distribution of the emission in PHA channels (cf. Fig. 3), we have found that the two sets of observations are consistent. A gain variation with time is expected to be responsible of the difference in the PHA distribution, as reported in the HRI calibration report (The ROSAT Users' Handbook) and therefore should not be indicative of an intrinsic change of the source characteristics. Since the details of the PHA distribution have not been exploited, rather the integrated PHA range has been considered, we have disregarded this difference and used the merged image for the analysis.

2.1. X-ray maps

Background subtracted X-ray images have then been obtained for all galaxies. To enhance different details, the raw data have first been binned and smoothed with Gaussian functions of increasing σ's. The results are described briefly below for each galaxy.

NGC 1553 The isointensity contour maps of Fig. 4 show that the emission from NGC1553 is complex and clearly deviates from azimuthal symmetry. The low resolution map is elongated along the optical major axis. At higher resolution, several features can be clearly identified: a "tail" is visible towards the SE; the central region appears elongated along the $\sim$ E-W direction, roughly perpendicular to the outer elongation and the optical PA. This is however further resolved in a possible spiral-like structure around the central peak, plus a more isolated, point-like source to the W (given the limited statistics the source could be consistent with a point-source). Two additional features can also be seen to the NW, at a distance of $\geq 1.'5$ from the center.

NGC 4649 As evident from the maps in Fig. 5, the X-ray emission from NGC4649 is regular and roughly azimuthally symmetric, as already shown by the PSPC data (Trinchieri et al 1996), and no significant features appear even at higher resolution.

Detailed X-ray Observations of Early Type Galaxies

G. Trinchieri[1] and L. Noris[2]

[1] Osservatorio Astronomico di Brera, Milano, Italy
[2] Università degli Studi di Milano, Milano, Italy

Abstract. The morphological distribution of the 10^7 K, x-ray emitting gas in two early type galaxies with complex, filamentary Hα emission is analyzed in detail and compared to the emission in the Hα line. The x-ray gas shows a structured, asymmetric, often clumpy emission at all scales. *Gross* similarities are observed between the Hα and x-ray morphologies, although there is not a one-to-one correspondence of the features present. The sample is much too small to allow us to draw conclusions and more examples will have to be analyzed before these similarities are interpreted as evidence of a common origin, or a common mechanism, linking the gas at different temperatures.

The study of different phases of the Interstellar Medium in early type galaxies has shown that, on average, galaxies with hot (10^7 K) gas also contain extended line emission observable in Hα (Trinchieri & diSerego 1991). In order to better understand this suggested relationship, we have programmed a detailed comparison between the emission at the two different wavelengths. For this we need: deep Hα images of galaxies with structured line emission that extends on scales $> 30'' - 1'$; and sensitive, high resolution x-ray observations of galaxies with hot gas. Only a handful of objects meet these requirements. At the present time we have analyzed two objects for this purpose: NGC 5846 and NGC 1553.

1. X-ray data

We have found that the high resolution observations of several early type galaxies indicate that the gas does not have a smooth, regular morphology, as was suggested by earlier, lower resolution observations, but often shows features and asymmetries. Whether this is a property of all early type galaxies when looked at in greater details is not clear at the present time and will require examination of a larger number of galaxies. In particular for the two galaxies under study:

NGC 5846: This galaxy has been observed both at high and low resolution with the ROSAT instruments. While the PSPC data (from the archive) only show asymmetric excess emission in the NE quadrant, the HRI observation clearly shows an elongated feature particularly prominent in the $1' - 3'$ galactocentric annular distance (Fig. 1). The emission also appears skewed, with a sharper decline to the west relative to the eastern emission. Some elongation towards the south could also be seen on a $1' - 2'$ scale. In the inner $1'$ radius the emission looks mostly azimuthally symmetric.

NGC 1553: This galaxy is fainter than NGC 5846 and the data are therefore of lower statistical significance. The HRI observation indicates that the emission at large scale is elongated along the NW-SE direction, similar to the optical Position Angle. On smaller scales, however, a change in PA is observed, and the emission appears elongated in the EW direction. A clear extention to the SE quadrant is also visible in the $30'' - 1.5'$ annulus. Opposite to the NW, some excess emission can also be seen at a distance of $1.5'$ from the peak (Fig. 2).

2. Hα images

Both galaxies present very structured Hα emission, extended on a scale of several $10''$.

NGC 5846: The emission is very filamentary and clumpy on all scales. A clear structured extention pointing to the North is visible in the NE quadrant (Trinchieri & diSerego 1991).

NGC 1553: In this galaxy as well the emission is very clumpy, with an overall elliptical shape oriented in a NW-SE direction. A clear tail extends to the SE, and clumps are also visible in the NW quadrant (Fig 2).

3. Comparison

It is clear that both the x-ray and the Hα images show complex morphologies. There is also a suggestion that they may be somewhat related. In **NGC 1553** there is a relatively good spatial coincidence between the Hα "tail" and the elongation in the x-ray data, and between the additional clumps observed in the NW quadrant at both frequencies. There is instead morphological similarity but no spatial coincidence in **NGC 5846**. In both images shown in Fig. 1 there is a clear elongation to the north in the NW quadrant. However, while the Hα emission is well within a radius of $1'$, asymmetries are only observed outside of this radius in the x-ray data.

At the present time we do not have enough information to understand whether these similarities are peculiar to these two objects, or whether they are indicative of a causal relationship between the two emissions. Data at other wavelengths, radio emission in particular, will also have to be taken into account, since a possible anticorrelation between radio and x-ray morphologies has been noticed in a few galaxies and clusters (*e.g.* NGC1399, Kim et al 1995). The presence of a radio structure could therefore affect both x-ray and Hα morphologies and could mask a more direct link between these two emissions. We will also have to examine a much larger number of objects with different line emission morphologies, both highly irregular and regular for a more comprehensive understanding of the relation between different phases of the ISM in early type galaxies.

References

Kim, D-W. et al 1995 ApJ in press

Trinchieri, G. & diSerego Alighieri, S. 1991, AJ 101, 1647

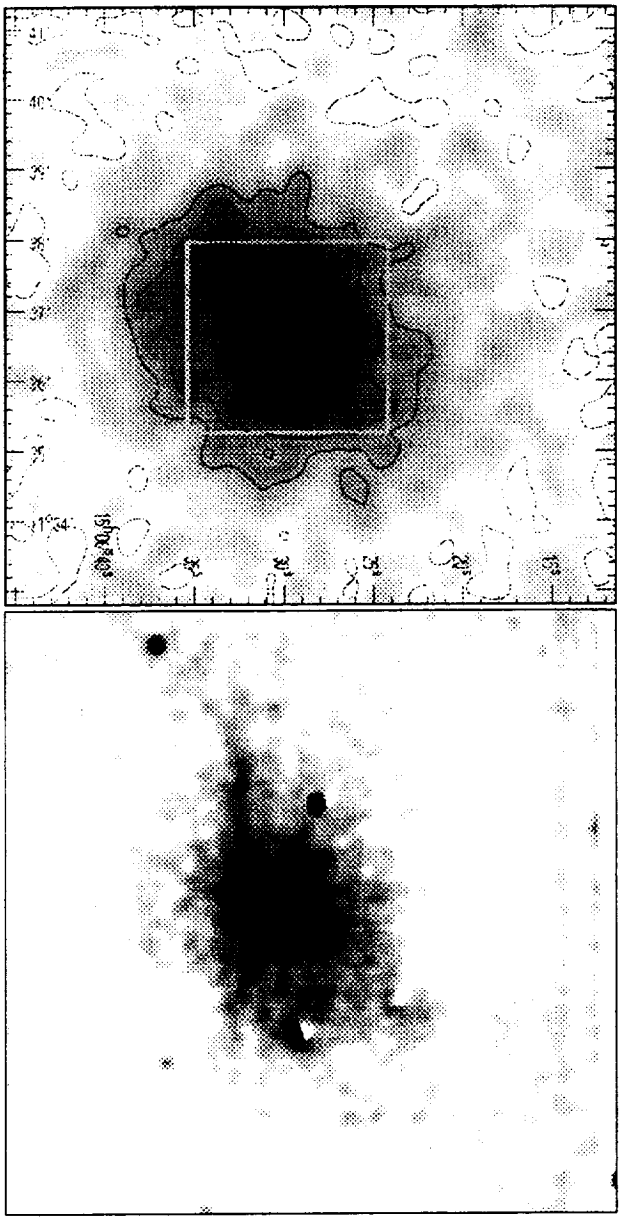

Fig. 1. X-ray (HRI; top; the image is binned to 3″ pixels and is smoothed with a gaussian function of $\sigma = 9''$) and Hα (bottom) images of NGC 5846. The Hα image covers roughly the area indicated by the box in the x-ray map

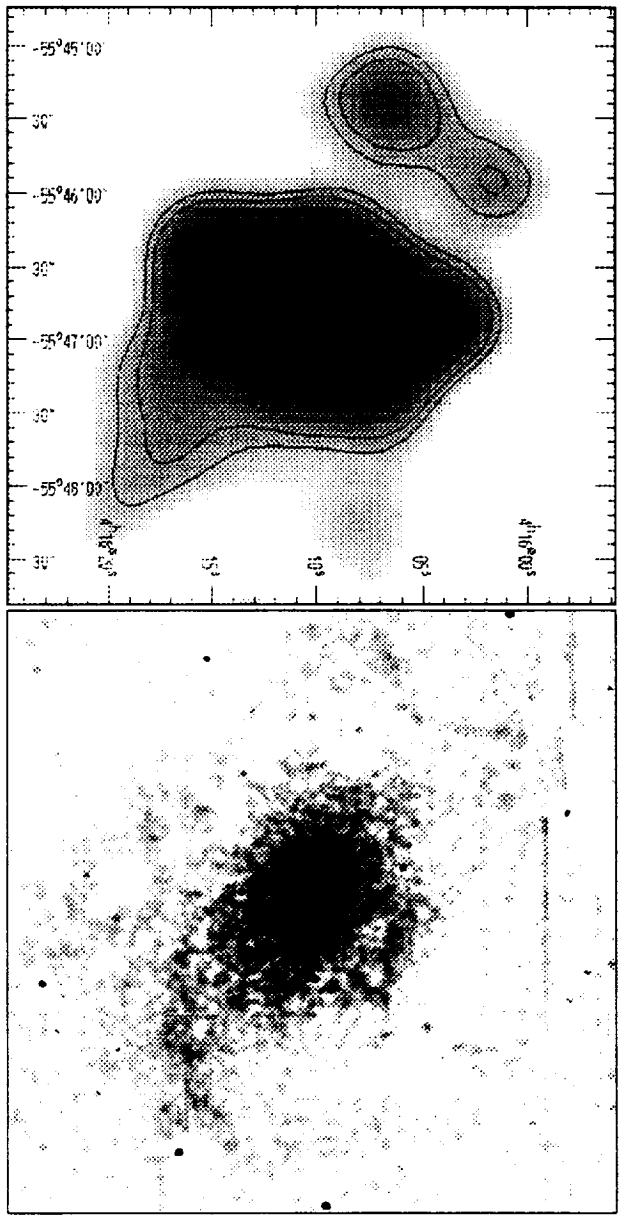

Fig. 2. X-ray (HRI; top; the image is binned to 4″ pixels and is smoothed with a gaussian function of $\sigma = 16''$) and Hα (bottom) images of NGC 1553. The two images are on the same scale

metric and clumpy. The elongation in the NE-SW direction that is visible in the low resolution image is clearly resolved in a feature extending in the NE quadrant, and most prominent at $1' - 2'$ radial distance from the peak (see Section 2.2 later and Fig. 7). At smaller radii the emission is also skewed, with a steeper gradient in the Western side (see Section 2.3). Several features can also be observed at small radii (smaller than $\sim 0.5 - 1'$), that can be described as clumps, holes and filaments. A more quantitative analysis of the reality of these features will follow.

DRAFT

2.2. Azimuthal profiles

The qualitative statements that the emission from NGC 1553 and NGC 5846 is not azimuthally symmetric have been checked more quantitatively by analyzing the azimuthal distribution of the emission. For all galaxies, we have divided in 8-10 azimuthal sectors the whole emission from the galaxy, namely a circle of radius 5′ for NGC 1553, and 7′ for NGC 4649 and NGC 5846. The results are plotted in Fig. 7. The azimuthal dependence of the emission is almost nonexistent for NGC 4649, while strong deviations from a constant are observed for the other two objects.

We have further analyzed the azimuthal distribution of their emission in concentric annuli, as described below for each of them. All angles are measured counterclockwise from North.

NGC 1553 . The 5′ region of the emission has been divided into 3 annuli of $0' - 1$; $1' - 3'$; $3' - 5'$ inner and outer radii respectively. Deviations from azimuthal symmetry are evident in all three annuli, although more evident in the $1' - 3'$ region. The "point source" to the W of the central region is visible in the $0' - 1'$ annulus at an angle of $\sim 240°$, while the $1' - 3'$ region shows the $\sim$ N-S elongation (see Fig. 4). A peak at $\sim 240°$ visible in the $3' - 5'$ annulus corresponds to the probably unrelated source visible in the SW quadrant.

NGC 4649 . As shown by Fig. 7, no significant deviations from the azimuthal symmetry are observed in this galaxy. A possible elongation towards the South, visible in the plot relative to the $0' - 7'$ annulus, is not evident at smaller radii.

NGC 5846 . The azimuthal distribution is divided in three annuli ($0' - 1'$, $1' - 2.'5$, and $2.'5 - 5'$) and is shown in Fig. 7. While the innermost $\sim 1'$ circle is relatively flat, and shows only the skewness of the emission to the W, the feature to the N is prominent in the $\sim 1' - 2.'5$ annulus (from $\sim 340°$ to $\sim 90°$). An extension to the S is also visible in the outermost annulus.

2.3. Radial profiles

The surface brightness distribution of the emission from each galaxy, obtained in concentric annuli, is shown in Fig. 8. As expected from the morphology of the emission discussed above, the radial profiles of all but NGC4649 are not smooth functions of radius. We have attempted to parameterize the radial profiles with a two parameter model ("King-type" model of the form $\Sigma_x \propto (1 + (\frac{r}{r_x})^2)^{(-3\beta+0.5)}$, with r_x as the core radius and β that indicates the radial dependence), To take into account the Point Spread Function (PSF) of the HRI, we have convolved the "King-type" model with the HRI PSF, as given by the "ROSAT HRI Calibration Report". However, we have obtained a reasonable fit only for NGC 4649, for which $r_x = 3''$ (consistent with values between $2''$ and $10''$) and β=0.47 $\pm$0.03.

For NGC 1553, a fit can be found outside $10''$, for a $r_x = 25''$ and β=0.41. Inside a radius of r=$10''$, there is a clear excess, probably due to an unresolved source.

To take into account the azimuthal asymmetry of the emission of NGC 5846, radial profiles in different pie regions and along different directions have also been obtained. Fig. 9 shows the comparison between the profiles obtained in the azimuthal limits from 85° to 340° and from 340° and 85°, where the feature to the N is visible. A significant excess in the $\sim 1' - 2.5'$ region is clearly seen. In fact, a fit to the 85° to 340° region (for $r_x = 15''$ and $\beta = 0.5$) is reported on the data and makes the excess quite visible.

2.4. Spectral data

All three galaxies have also been observed with the ROSAT PSPC, as indicated in Tab. 1. A detailed analysis of the PSPC data of these objects is beyond the purpose of this work. However, the spectral information that is contained in the PSPC data is useful to derive fluxes and luminosities and to better study the characteristics of the ISM in these galaxies. We have therefore obtained the PSPC data of NGC 1553 and NGC 5846 from the ROSAT archive to analyze them. NGC 4649 results have been taken from Trinchieri et al (1996). The analysis is done using the IRAF-PROS

galaxies (Trinchieri et al 1994; 1996).

In order to estimate the total extent of the emission in the PSPC we have produced a radial distribution of the 0.2-2 keV photons binned in concentric annuli about the peak of the X-ray source, and compared it with the radial distribution of the data contained in the exposure map, that simulates the spatial response of the instrument to a constant incident source with a characteristics temperature of 1 keV. The unrelated sources that are also detected in the fields have been masked out in this comparison. Since the two radial distributions appear very similar at radii of $7'$ and $> 12'$ for NGC 1553 and NGC 5846 respectively, the region of the field outside these radii can be used to estimate the background (see also Trinchieri et al. 1994, 1996). To minimize the effect of vignetting, an annulus as close as possible to the source will be used to estimate the background. For NGC1553 the $7' - 10'$ annulus appears free of sources and can be used for this purpose. For NGC5846 however, in order to avoid the circular support structure of the PSPC, the annulus at $25' - 27'$ has been used.

To estimate the gas temperature, we have assumed a thermal plasma model (Raymond-Smith code) with cosmic abundances and low energy absorption.

DRAFT

NGC1553 . We have obtained the spectral distribution of the counts in the whole $7'$ circle and in the inner $2'$ region. To these, a properly rescaled and vignetting-corrected background has been subtracted (see PROS documentation). A one temperature spectral fit to both regions does not give a satisfactory result: the best fit χ^2 value is high and the best fit low energy absorption would imply a column density much lower than the line-of-sight value of 2.4×10^{20} cm^{-2}. Fixing the low energy absorption at the line-of-sight N_H column results in even poorer fits. The spectrum also seems much harder than usually found in bright early type galaxies (see Tab. 2).

We have therefore tried a two component fit, using two Raymond-Smith models with cosmic abundances. As shown by the Table, this reduces significantly the best fit χ^2 value, and suggests that a very soft ~ 0.1 keV and a harder $\sim$ 1 keV plasma could describe the data, when the absorbing column is fixed at the galactic value. The two components appear to contribute similar amounts in the inner $0' - 2'$ circle, while the $\sim$ 1 keV component contributes $\sim$ 60% of the total extended emission.

NGC5846 . The source region of NGC 5846 has been divided into 3 concentric annuli, and a spectral fit has been done on each. We have used two separate background estimates: the $25' - 27'$ region and the adjacent outer annulus, in an attempt to subtract in part the contribution from the outer regions that are projected onto the innermost part (a proper procedure would require a more sophisticated spatial/spectral deconvolution of the data). The results are summarized in Tab. 3.

It is evident that the gas is cooler in the inner regions, as found in other early type galaxies (cf. Trinchieri et al. 1996), and that the temperature is an increasing function of radius. This evidence is stronger when the "local" background is subtracted to the data, even though the statistics are poorer.

However, while the average temperature in the annulus might be an increasing function of radius, the presence of substructure suggests that the average value might not apply everywhere in the annulus. For example, a significant feature is present in the $1' - 2.'5$ annulus, where enhanced emission is clearly observed in the HRI data to the NNE (Fig. 6). We have therefore checked whether the observed enhancement corresponds to different spectral characteristics of the emission.

We have divided the $1' - 2.'5$ annulus in two separate regions, one comprised between the angular limits $85° - 340°$ and the other in the complementary region, and measured the spectral characteristics of the two regions separately. The background is estimated in the $2.'5 - 4'$ annulus. For the $340° - 85°$ sector we have also used as background the $85° - 340°$ region at the same radial distance. The results are summarized in Table 3.

The region of the filament is cooler than the rest of the annulus, with kT$< 0.76 - 0.78$ keV compared to kT> 0.76 keV (90% values).

2.5. Fluxes, luminosities and densities of the hot gas

The spectral results above have been used to derive the luminosity of the sources associated with these galaxies and to estimate the emission from the substructures in NGC1553 and NGC5846. We have used the best fit spectral parameters to convert from HRI count rates to 0.2-2 keV fluxes. Luminosities are derived from the assumed distances of 21.5, 17 and 45.8 Mpc, for NGC 1553, NGC 4649 and NGC 5846 respectively.

Gas densities can also be derived in different regions. However, as already extensively discussed elsewhere (see Trinchieri et al 1996 and references therein), a number of assumptions have to be made on the state of the gas and

serious assumption relates to the volume assumed to derive gas densities, since the emission is clearly clumpy and structured. In Fig. 10 we show the density profiles derived for the three galaxies from the average surface brightness profiles obtained in Section 2.3, deprojected under the assumption of spherical symmetry (Kriss et al 1993), for the average temperatures derived in Section 2.4. For NGC 1553, for which a two temperature model is required, we have used kT =1.008 keV (the value of the high temperature component). The innermost point in NGC 1553 is probably dominated by the point-like source, and should therefore be disregarded for the purpose of central density estimates. The total amount of hot gas in these galaxies is $M_{gas} \sim 0.4 - 4 \times 10^{10}$ $M_{\odot}$, and cooling times are shorter than $\sim 10^{10}$ yr out to the outermost radius used in these estimates, and are $10^7 - 10^8$ yr in the innermost regions.

Given the clumpy nature of the emission however we expect that locally the gas could have significantly different densities than those derived on the average at different radii. We have estimated the density in two regions: the tail of NGC 1553 and the NNE feature of NGC 5846 (see Tab. 2 and Tab. 3). To estimate the volume occupied by the gas, we have assumed a cylinder. For NGC 1553, the height h of this cylinder and the radius of the base b are h=2.6 and b=6.8 kpc. The density in this regions is therefore $n_e \sim 0.01$ cm^{-3}. For NGC 5846, assuming $h = 1.'5$ and $b = 0.'3$ for the cylinder, $n_e \sim 0.025$cm^{-3}. Although these numbers should be taken with caution, since their estimate relies heavily on the volume assumed, the local densities could be ~ 10 times higher than the average value derived at the same radial distance (see Fig. 10).

DRAFT

3. Comparison between X-ray and Hα Emissions

Hα maps of these galaxies have been obtained with the 3.6 meter and the NTT at ESO. The analysis of these data is presented elsewhere (Trinchieri & diSerego 1991; diSerego et al 1996). Here we use those observations for a comparison with the X-ray maps.

Two of the galaxies analyzed here, NGC 1553 and NGC5846, show a very structured Hα morphology. In both cases, the emission is not azimuthally symmetric, and filaments and substructures can be clearly identified. Emission out to a radial distance of r $\sim 40''$ (not including the fainter filaments the the SW and to the NW) for NGC 1553 and r $\sim 30''$ (not including a filament extending north in the NW quadrant) for NGC5846 is visible. On the contrary, the Hα map of NGC 4649 shows little deviations from azimuthal symmetry, is centrally peaked and extends out to a radius of r$\sim 30''$ (Fig. 11, 12, 13).

As already discussed in the previous sections, structures are also observed in the X-ray emission of NGC 1553 and NGC5846, while the map of NGC4649 shows a more regular, azimuthally symmetric morphology.

NGC 1553 The comparison between the X-ray and Hα maps is shown in Fig. 11. The Hα map enhances the low surface brightness features at larger radii, for a more significant comparison with the X-ray data. At smaller radii the Hα image shows a central peak with an elongation and spiral structure along the NS direction, but this structure is confined in the inner $\sim 8''$, where the comparison with the X-ray data is very difficult, both because of the poorer spatial resolution and limited statistics, and because of the presence of a central source in the X-ray data as well. At larger radii, a more diffuse, elliptical Hα morphology can be seen, resembling the stellar light, that extends in a sort of a faint tail to the SE. A similar feature at the same radial distance from the peak is observed in the X-ray emission as shown by Fig. 11. Two filaments to the NW, at a radial distance of $1.'5$ from the central peak, are spatially coincident with two features in the X-ray map.

NGC 4649 As already discussed by Trinchieri & diSerego (1991) the line emission from NGC4649 is centered on the nucleus and extends in a roughly azimuthal symmetry out to r$\sim 30''$ (Fig. 12). The X-ray map also shows azimuthal asymmetry both in the same area covered by the line emission (Fig. 12) and out to a larger scale of r$\sim 7'$.

NGC5846 Complex line emission peaked on the nucleus with a filamentary structure visible in particular in a clear finger-like feature in the NE quadrant is observed in NGC 5846 (Fig. 13). Several of the Hα features seem to have a correspondence in the X-ray morphology, even though often this is more a qualitative than a quantitative statement. In particular, the Hα filament to the NE has a corresponding feature in the same quadrant and similar direction in the X-ray map. The scale of the X-ray feature is however not the same as the Hα: while this latter is visible at $30''$ to $60''$ from the central peak, the X-ray feature begins at $\sim 60''$, and extends out to $\sim 2' - 2.'5$. On smaller scales, there is not a coherent structure in the X-ray map, although excess emission starts at $\sim 30''$ in the NNE quadrant (see Fig. 9).

The intriguing observational results of a spatial correlation between X-ray and Hα features in the central regions of early-type galaxies need to be understood. It is common belief that the X-ray emission in X-ray bright early-type galaxies is dominated bye the radiation of the hot interstellar medium. The characteristics of this gas indicate that it can cool on short timescales, and more so in the denser, cooler central regions. The line emission is somewhat more complicated to understand, in particular if associated with the hot gas. Originally it was suggested that the the Hα filaments observed in several cooling flow clusters could originate directly from the cooling of the 10^7 K gas. By analogy, this mechanism would also work in early-type galaxies. However the expected intensity of the lines, for reasonable assumptions of the recombination rate, is significantly below the values observed (Johnstone et al 1987, Trinchieri & diSerego 1991, Heckman Baum ...). Trinchieri & diSerego (1991) proposed that the stellar population, in particular the Post Asymptotic Giant Branch stars, might provide enough ionizing photons to explain the observed emission. While properly accounting for the energetic requirement, such a mechanism would not explain however the peculiar morphology of some of these systems, since the ionizing photons are expected to be evenly distributed in the galaxy (in particular they would follow the stellar distribution), nor would it explain the close connection between very hot and warm gas. A peculiar gas distribution would have to be introduced, to explain the observed morphologies.

Sarazin et al ... and Kim et al have suggested that the radio sources found in galaxies and cluster would influence the distribution of the gas. Anticorrelation between the radio jets and X-ray emission is observed in NGC 1399 and While this could explain the cases above, neither NGC 1553 nor NGC 5846 are known to host structured radio sources. In fact, only NGC4649, that shows no peculiar morphology in either Hα or X-ray, shows a weak radio jet (Stanger XXX). Therefore it is likely that a more direct link between hot and warm gas is required to explain the observed similarities.

Two models have been proposed that would provide a link between these two gas phases. DRAFT

Voit & Donahue (1990) and Donahue & Voit (1991) present a theoretical model based on the assumption that the optically emitting filaments are powered by the radiation from gas emitting in the X-rays and EUV that predicts a high efficiency for converting soft X-ray photons into optical line emission, and therefore is able not only to reproduce the line ratios observed, but also to account for the high luminosity of the optical emission lines. However, the feasibility of the model has more recently been questioned.

Sparks et al. (1989) suggest that heat transfer from the X-ray gas to the dust, often found associated with these optical line filaments, might provide the excitation for the line emission. Their model, applied to the data of NGC 4649, explains their observations quite well.

As already discussed, we do not require a *source* of ionizing photons in early type galaxies, but we do need to explain the peculiar morphologies found. Since the ionizing field is expected to be more homogeneously distributed throughout the galaxy, we can assume that the peculiar morphologies reflect a peculiar distribution of the gas. We expect that the bulk of the hot gas is produced by the mass loss from stars, and it should therefore also reflect the optical light distribution. The origin of the cold gas is however less definite: it could also come from the stellar mass loss, it could have been accreted from outside (through mergers for example) or it could come from the cooling of the hot gas.

Two scenarios can be explored to explain the peculiar morphology of the cold gas, independent from the hot gas: tidal forces, resulting from interaction with other galaxies or from a merging event; internal forces (*e.g* magnetic fields, radio structures) that modify the more regular gas distribution. This latter would not work in these systems, as discussed above. Tidal forces could be invoked to explain the peculiar gas distribution of NGC 1553, known to be interacting with NGC1549. However, NGC 5846 is at the center of a small group and should not be interacting. Merging with a smaller group member cannot be dismissed, even though no other obvious signs of such event are observed in the optical.

However, even if we assume "as given" that the cold gas has the observed morphology (through one of the scenarios discussed above, for example), we are still left with the question of how and why cold and hot gas (or at least some of the hot gas) have similar distribution. We could then consider a third component of the interstellar medium of these objects, quite often associated with the cold gas: dust. Dust has been observed in early type galaxies both through their far infrared emission (Jura) and from direct observations of obscuring material in the optical. Dust can be quite efficient in cooling the hot gas (see Cowie and Mckee 1977). We can therefore expect excess X-ray emission resulting from heat conduction to the cold dust. As shown by the map of Trinchieri & diSerego (1991), there are two dust filaments in NGC 5846, one of which is in the general direction of the feature in the NE quadrant. Moreover, recent observations by Goudfrooij ... indicate that the dust is probably coextensive with the Hα emission, and could therefore act as a cooling agent throughout the region where the Hα and X-ray peculiar morphologies are observed. Dust is also observed in the central region of NGC 1553 (diSerego et al 1996).

5. Conclusions

DRAFT

The high resolution images of some high X-ray luminosity early type galaxies reveal the presence of inhomogeneities and structures in the gas morphology. These features appear both as (positive or negative) clumps in a more diffuse emission, on scales of a few arcsec, and as more coherent structures such as filaments/tails on scales of the order of arcminutes. PSPC spectral data of NGC 5846 indicate a significantly cooler temperature in one such feature, which suggests a $\sim$ 10 times denser medium in the area.

A suggestive analogy is found between features in the Hα and X-ray maps of NGC 1553 and NGC 5846, while NGC 4649 shows no significant structures at either wavelengths. This suggests that a link exists between these two phases of the gas, that determines the spatial distribution of the emission. While confinement from radio structures does not seem to provide a good explanation for these objects, a possible link through heat conduction from hot gas to dust that gives rise to Hα features provides a reasonable explanation and accounts for energetics and spatial coincidence of these three components of the interstellar medium.

Acknowledgements. This work was supported by the Agenzia Spaziale Italiana (ASI) and by NASA grant NAG5-2049 (ROSAT). This research has made use of the NASA/IPAC Extragalactic Database (NED) which is operated by the Jet Propulsion Laboratory, California Institute of Technology, under contract with the National Aeronautics and Space Administration.

References

Kriss, G.A., Cioffi, D.F. & Canizares, C.R. 1983, ApJ 272, 439.
Tody D. 1986, in Instrumentation in Astronomy VI, ed. D.L. Crawford (Proc. SPIE, vol. 627) 733.
Trinchieri, G., Kim, D-W., Fabbiano, G., & Canizares, C.R.C. 1994, ApJ 428, 555
Trinchieri, G., Fabbiano, G., Kim, D-W., 1996, AA, in press
Trümper, J. 1983. Adv. Space Res. 2, No. 4, 241.
Worral, D.M. et al. 1992, in Data Analysis in Astronomy IV, ed. V. di Gesù et la. (New York: Plenum), 145.

Table 1. Log of the HRI and PSPC observations

Name	R.A. optical (J2000)	Dec.	begin/end	Observing Time (sec)	Instrument
NGC 1553	04 16 10.4	−55 46 51	14/06/94-26/08/94	46148.5	HRI
			19/08/93-24/09/94	15320	PSPC
NGC 4649	12 43 40.3	+11 32 58	11/07/94-11/07/94	2195.8	HRI
			17/06/95-18/06/95	11826.7	HRI
			21/12/91-27/12/91	14301	PSPC
NGC 5846	15 06 29.4	+01 36 25	02/02/94-05/02/94	22581.0	HRI
			05/08/94-11/08/94	16763.4	HRI
			25/07/92-05/08/93	8808	PSPC
			18/01/93-18/01/93	5947	PSPC

This article was processed by the author using Springer-Verlag LaTeX A&A style file *L-AA* version 3.

Table 2. Spectral characteristics of the emission in NGC 1553

Region	net counts and error	N_H	kT_1	90% conf. limits	kT_2	90% conf. limits	Normal. ratios[1]	χ^2_{min}	DOF	Notes
$0' - 2'$	980±38.6	18	3	> 2				47.5	22	A,B,C
		20.38	3					182.3	23	C,D
		20.38	0.133	0.115-0.155	1.057	0.90-1.45	-0.044	34.8	20	D
		18.00	0.308		3.0		0.732	13.9	20	A,B
$0' - 7'$	1587.6± 76.9	18	3	> 2				61.2	22	A,B,C
		20.38	3					149	23	C,D
		20.38	0.139	0.11-0.16	1.008	0.70-1.20	-0.195	31.2	21	D
		18.00	0.276		2.48		0.505	15.4	20	A

DRAFT

Notes:

1 Ratio between the normalization parameter of second component relative to the first (log ($norm_2/norm_1$)).
A The program finds the lowest value in the allowed range of N_H values.
B The 90% upper limit to the galactic absorption, for 2 interesting parameters, is ~ 19.5
C The program finds the uppermost value in the allowed kT range.
D The N_H parameter has been fixed at the galactic value

Table 3. Spectral characteristics of emission in NGC 5846

Region	net counts and error	N_H	90% confidence limits	kT	90% confidence limits	χ^2_{min}	DOF	Notes
$0' - 1'$	2604.1±56	20.40	20.25-20.55	0.604	0.54-0.65	30.9	20	A
	2110.3±57	20.45	20.30-20.60	0.561	0.50-0.62	22.8	20	B
$1' - 2.'5$	2611.9±58.4	20.37	20.25-20.50	0.810	0.77-0.84	30.0	21	C
	2158.9±62.4	20.35	20.20-20.50	0.780	0.72-0.83	25.0	21	B
$2.'5 - 5'$	1161.6±53	20.52	20.20-21.00	0.959	0.90-1.06	26.2	21	
	848.6±55.0	20.50	20.10-21.5	0.996	0.86-1.12	19.1	21	B
$5' - 12'$	1857.0±132.3	20.01	-	0.803	0.60-0.96	46.15	21	D
$0' - 5'$	6396.62±94.3	20.36	20.25-20.50	0.752	0.73-0.79	78.2	22	E
	5982.7±96.6	20.34	20.25-20.45	0.747	0.72-0.78	61.7	22	B,F
.....								
$1' - 2.'5$								G
$85° - 340°$	±	20.34	20.10-20.60	0.818	0.76-0.88	8.7		
$340° - 85°$	±	20.105	<20.40	0.710	0.62-0.78	17.7		
$340° - 85°$	±	20.13	< 21	0.577	0.36-0.76	10.5		H

NOTES: The background is obtained from the $25' - 27'$ annulus, unless otherwise noticed.

A The χ^2_{min} is reduced to 16.8 if a two temperature model is adopted. The best fit parameters are: N_H=20.51; kT_1=0.554; kT_2=3 (Upper limit of the allowed range)
B The background is obtained from the adjacent annulus (of $1' - 2'$; $2.'5 - 4'$; and $5' - 9'$ inner and outer radii).
C The χ^2_{min} is reduced to 18.9 if a two temperature model is adopted. The best fit parameters are: N_H=20.45; kT_1=0.745; kT_2=3 (Upper limit of the allowed range)
D The χ^2_{min} is reduced to 25.5 if a two temperature model is adopted. The best fit parameters are: N_H=20.48; kT_1=0.674; kT_2=3 (Upper limit of the allowed range)
E The χ^2_{min} is reduced to 25.4 if a two temperature model is adopted. The best fit parameters are: N_H=20.46; kT_1=0.675; kT_2=2.9
F The χ^2_{min} is reduced to 24.7 if a two temperature model is adopted. The best fit parameters are: N_H=20.49; kT_1=0.365; kT_2=1.7
G The $1' - 2.'5$ annulus is divided into the two angular regions. The background is obtained from the $2.'5 - 4'$ annulus.
H The background is obtained in the $1' - 2.'5$ region, with the exclusion of the $340° - 85°$ sector.

Table 4. Fluxes and luminosities for the galaxies and their components

Galaxy	RA (J2000)	Dec (J2000)	Radius "	net counts	error	flux ($\times 10^{13}$) erg cm^{-2} s^{-1}	Luminosity erg s^{-1}	Notes
NGC 1553	4 16 10.3	-55 46 48	300	2132.4	137.4	26.0	1.44×10^{41}	HRI; A
			420	1587.6	76.9	19.6	1.08×10^{41}	PSPC
central source	4 16 10.3	-55 46 48	15	203.4	17.0	2.48	1.37×10^{40}	
N. feature 1	4 16 06.5	-55 45 24	20	38.0	11.0	0.46	0.26×10^{40}	B
N. feature 2	4 16 01.5	-55 45 54	20	36.6	11.0	0.45	0.25×10^{40}	B
unrel. P. S.	4 16 03	-55 46 54	15	29.6	9.6	0.36	0.20×10^{40}	C
central diffuse	4 16 11.5	-55 46 52	80×120	332.4	26.4	4.05	2.24×10^{40}	D
tail feature	4 16 17.5	-55 47 50	50×65	50.9	17.7	0.62	0.34×10^{40}	E
NGC 4649	12 43 40	11 33 10	420	2346.4	132.8	43.7	1.52×10^{41}	HRI
			420	5890	103	46.2	1.61×10^{41}	PSPC; F
NGC 5846	15 06 29.2	1 36 24	420	8508.9	250.6	69.2	1.74×10^{42}	HRI
			300	5982.7	96.6	50.6	1.27×10^{42}	PSPC
NNE feature			(60-150)	688	53	5.19	1.31×10^{41}	G

NOTES: No correction is applied to the flux estimate to account for photons scattered outside the source region. Fluxes are estimated using the best fit parameters obtained in section 2.4 (see Tab. 2 and 3). HRI/PSPC indicate the instrument used to derive the total flux.

A The source at 4:16:51 -55:49 has been masked out

B The background is obtained in the annulus at the same radial distance from the peak (excluding the regions occupied by the two sources).

C The background is obtained from the Eastern half of the adjacent 20″ – 100″ annulus

D The counts are obtained in a 80″ × 120″ box. The background is obtained in the adjacent rectangular annulus with outer dimensions of 160″ and 240″.

E The background is obtained in the Southern half of the rectangular annulus concentric to the box, and with 45″ – 80″ inner and outer radii respectively.

F From Trinchieri et al. (1996)

G Excess counts in the 340° – 85° sector of the 1′ – 2.′5 annulus, above the average emission in the 85° – 340° at the same angular distance.

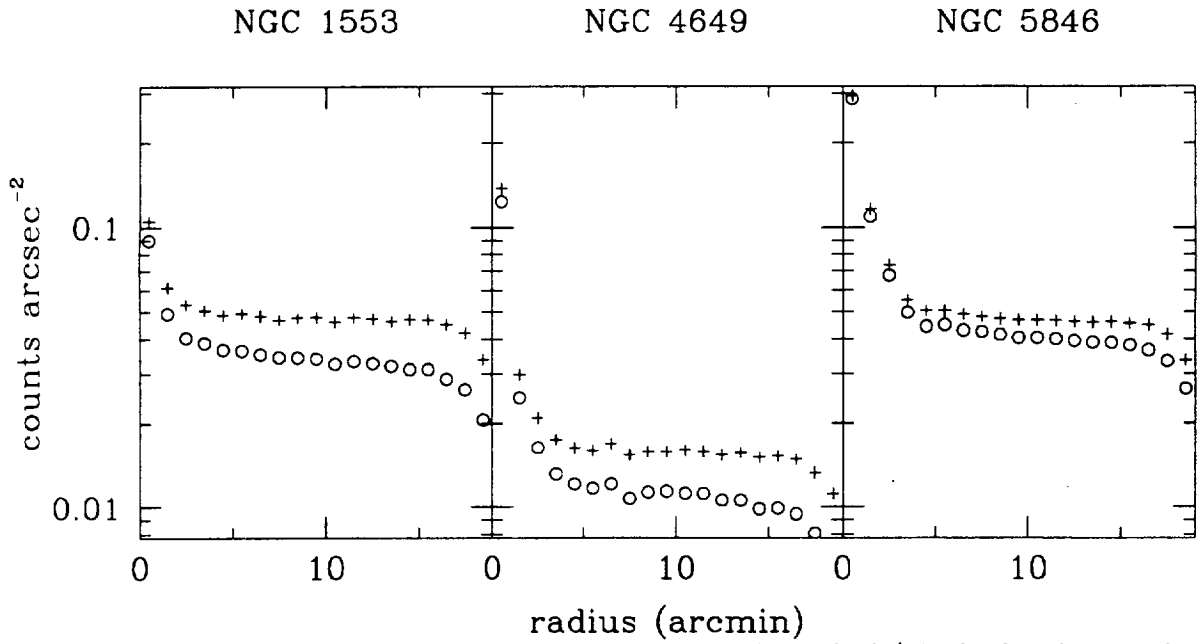

Fig. 1. Radial distribution of the detected photons binned in concentric annuli of 1′ size for the galaxies in the present sample. Crosses indicate the entire PHA range, dots are for the selected PHA range (see text).

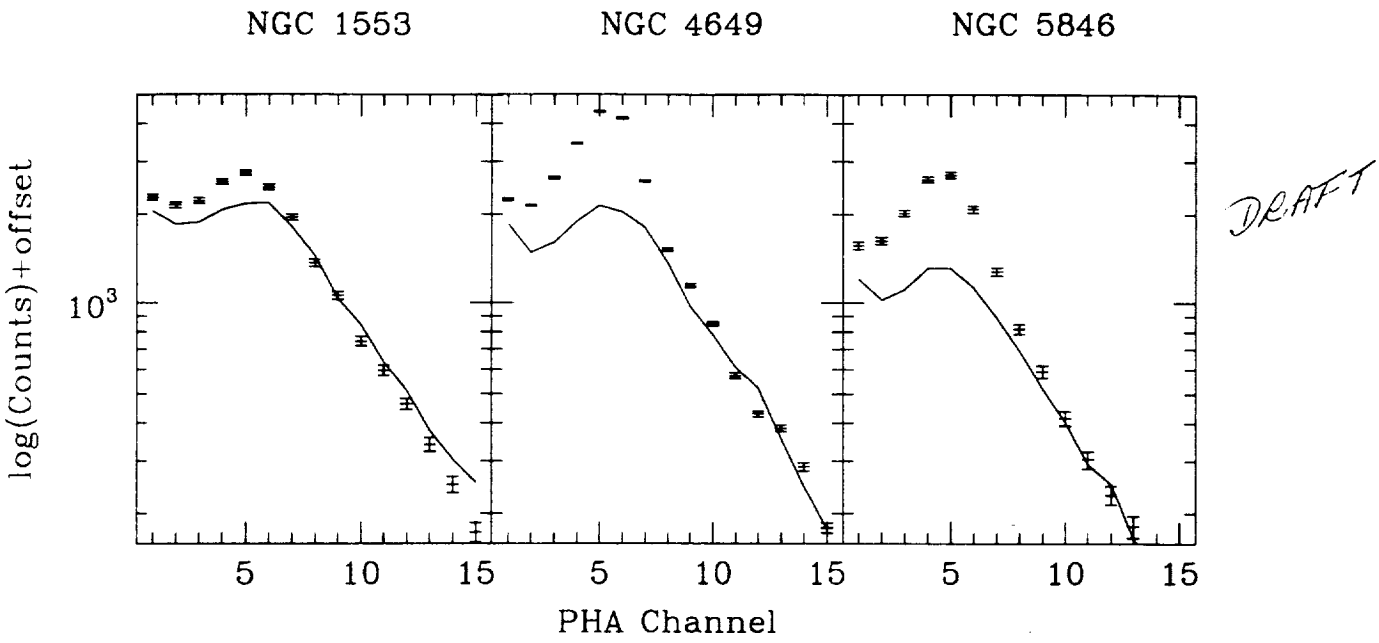

Fig. 2. PHA distribution of the photons in the "source" and in the "background" regions. The "source" region is a circle of radius r=5′, 7′, and 7′ for NGC 1553, NGC 4649 and NGC 5846 respectively. The "background" is extracted from an annulus at 8′ – 10′

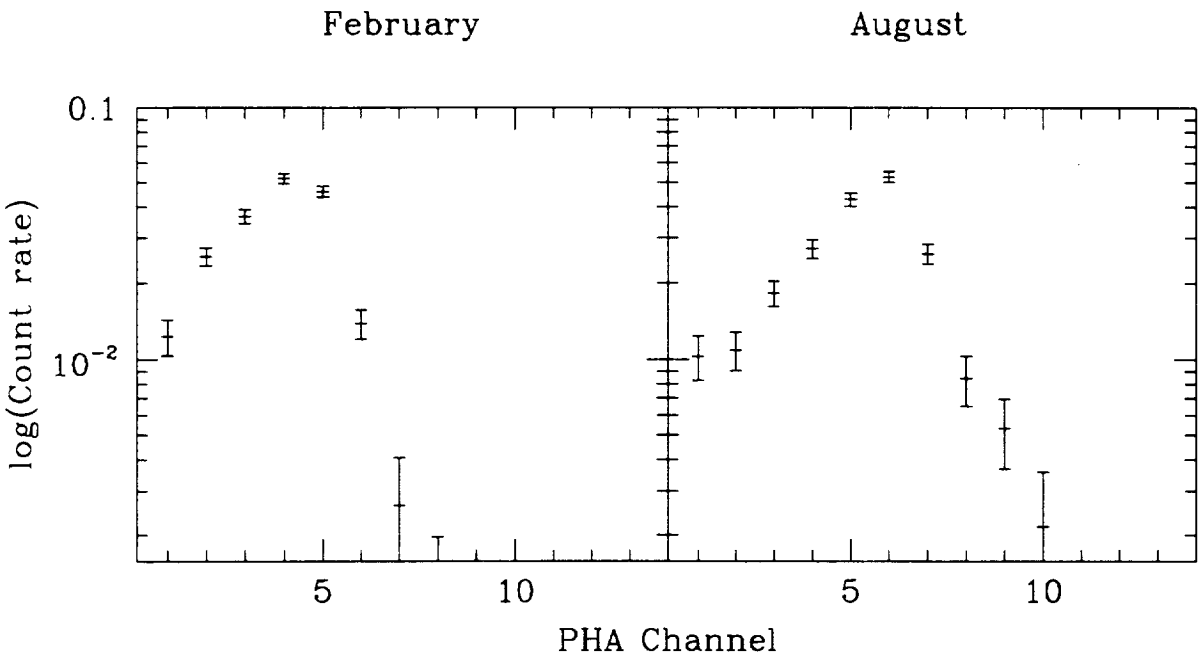

Fig. 3. PHA distribution of the net count rate extracted from a circle of 5′ radius in the February (left) and August (right) observations of NGC5846

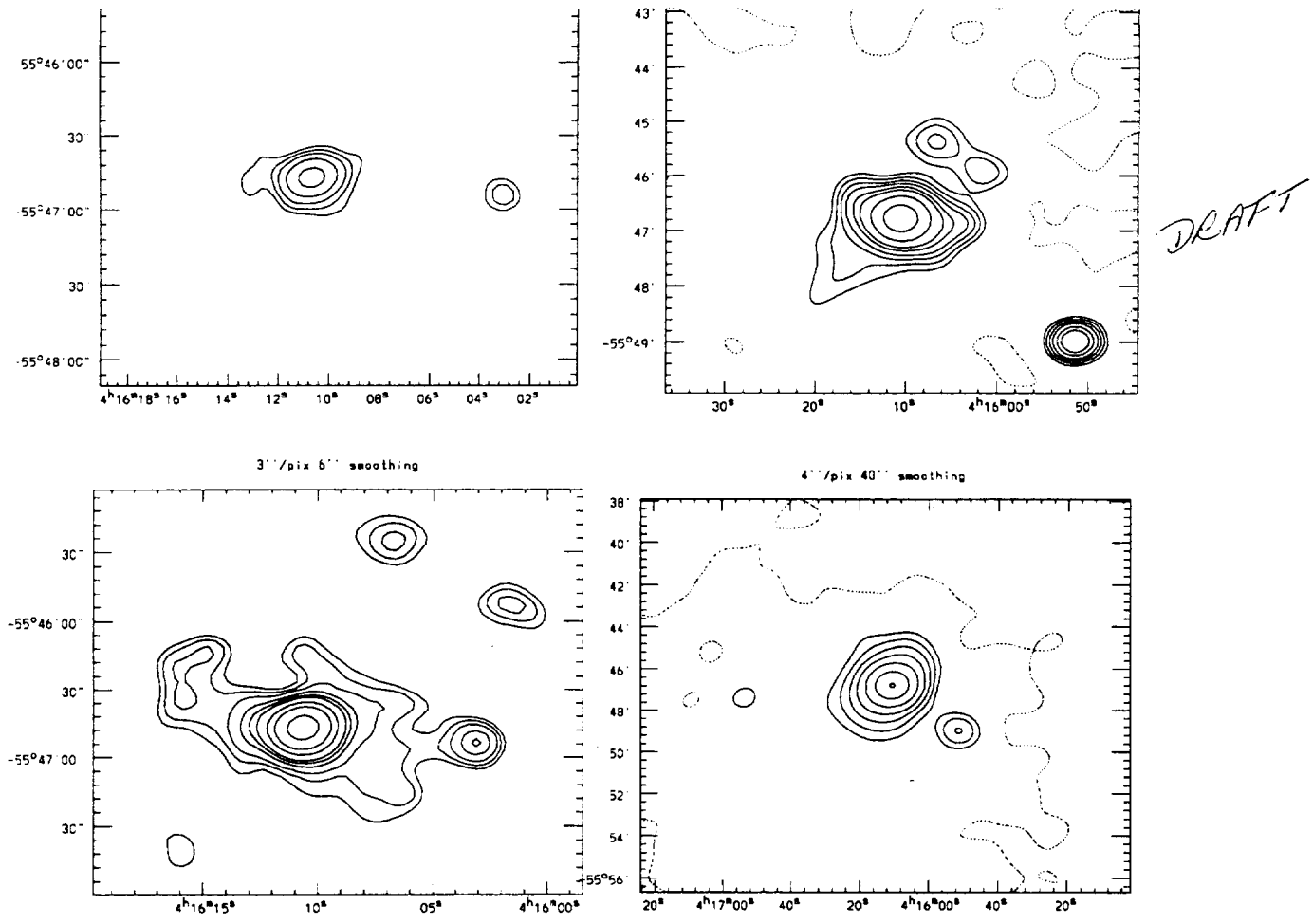

DRAFT

Fig. 4. Isointensity contour maps of NGC 1553, obtained with Gaussian smoothings of different sizes, as specified.

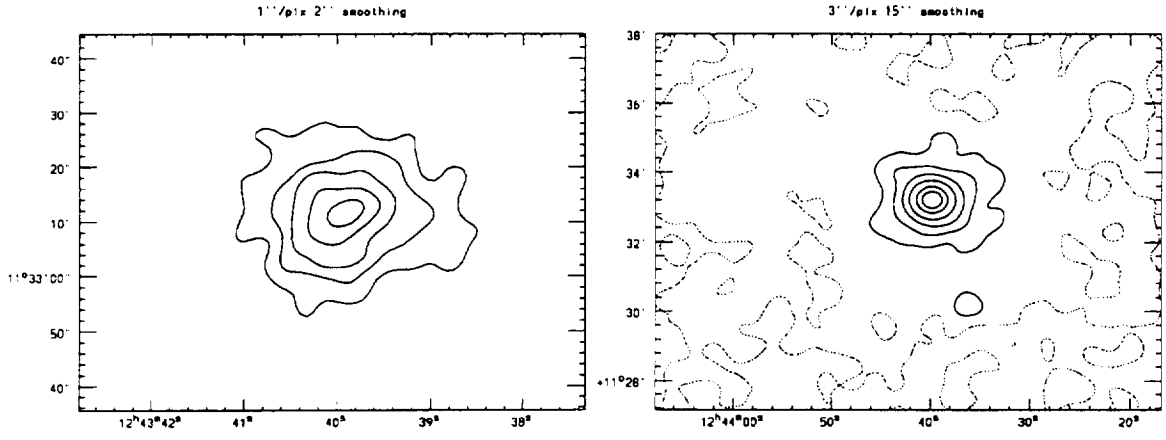

Fig. 5. Isointensity contour maps of NGC 4649, obtained with Gaussian smoothings of different sizes, as indicated. Contour levels are ...

DRAFT

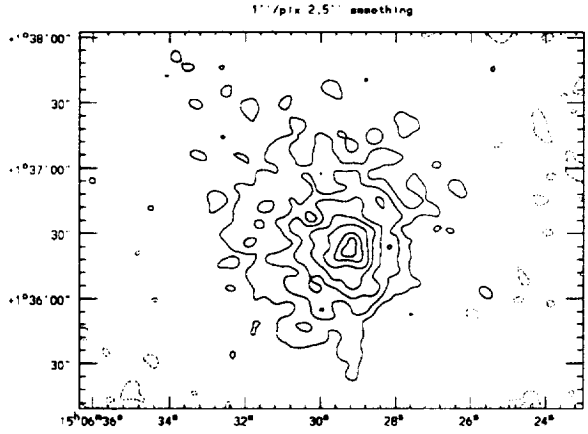
1''/pix 2.5'' smoothing
+1°38'00"
30"
+1°37'00"
30"
+1°36'00"
30"
15h06m36s
34s
32s
30s
28s
26s
24s

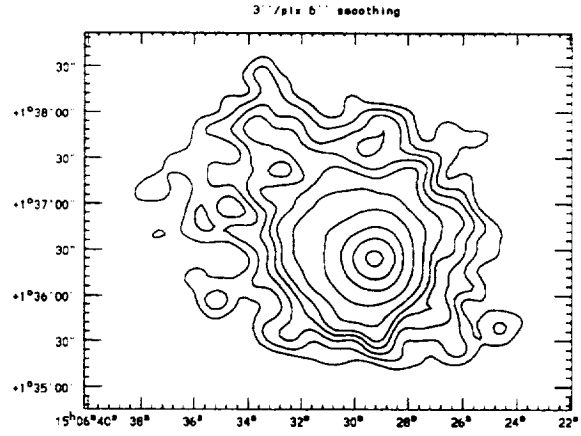
3''/pix 6'' smoothing
30"
+1°38'00"
30"
+1°37'00"
30"
+1°36'00"
30"
+1°35'00"
15h06m40s
38s
36s
34s
32s
30s
28s
26s
24s
22s

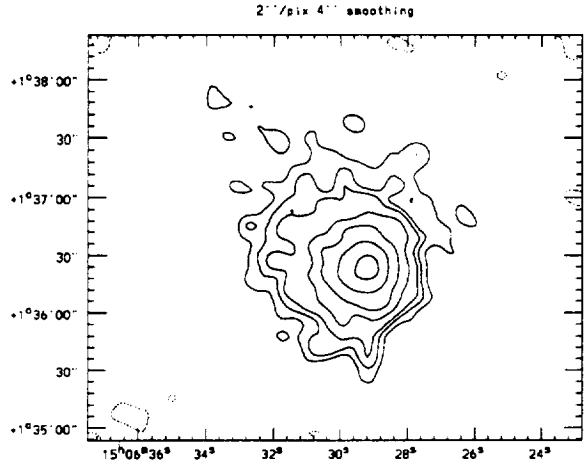
2''/pix 4'' smoothing
+1°38'00"
30"
+1°37'00"
30"
+1°36'00"
30"
+1°35'00"
15h06m36s
34s
32s
30s
28s
26s
24s

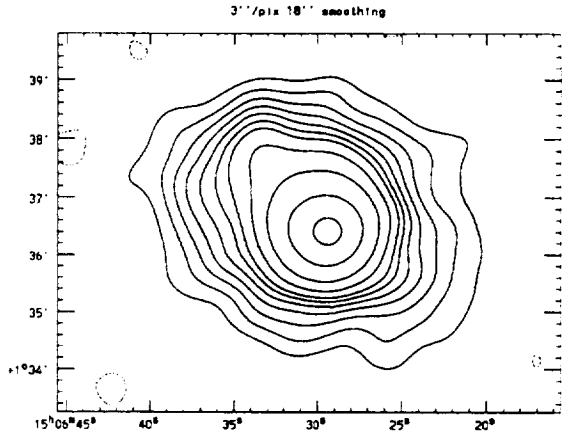
3''/pix 18'' smoothing
39'
38'
37'
36'
35'
+1°34'
15h06m45s
40s
35s
30s
25s
20s

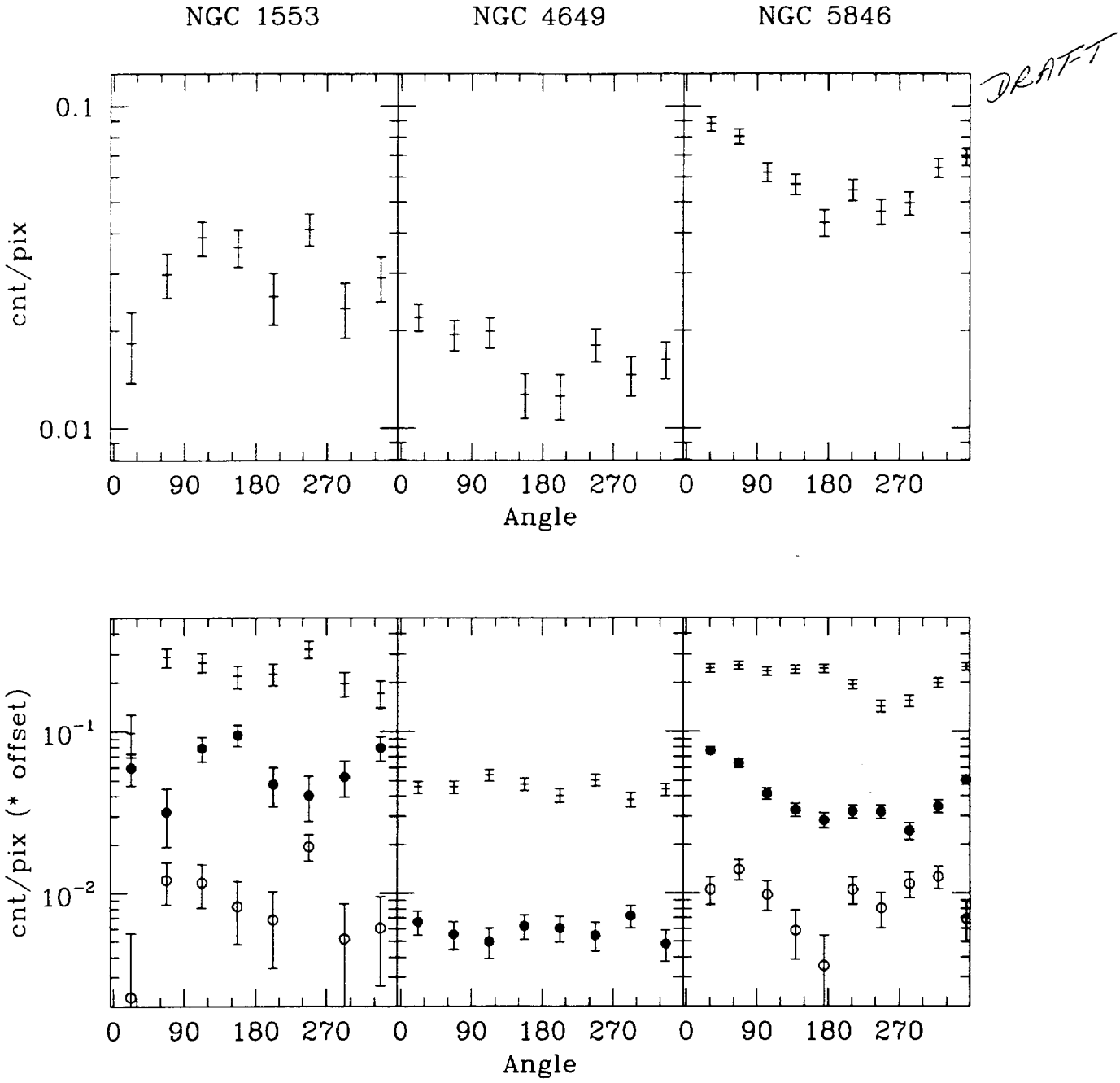

Fig. 7. Azimuthal distribution of the emission within a circle of 5′ (NGC1553) and 7′ (NGC4649 and NGC5846) is shown in the upper panel. In the lower panels, the azimuthal distribution in different annuli is plotted. Crosses are for the $0' - 1'$ annulus, filled dots for the $1' - 3'$ (NGC 1553 and NGC 4649) and $1' - 2.'5$ (NGC 5846) annuli; and open dots for the $3' - 5'$ (NGC 1553) and $2.'5 - 5'$ (NGC 5846) annuli.

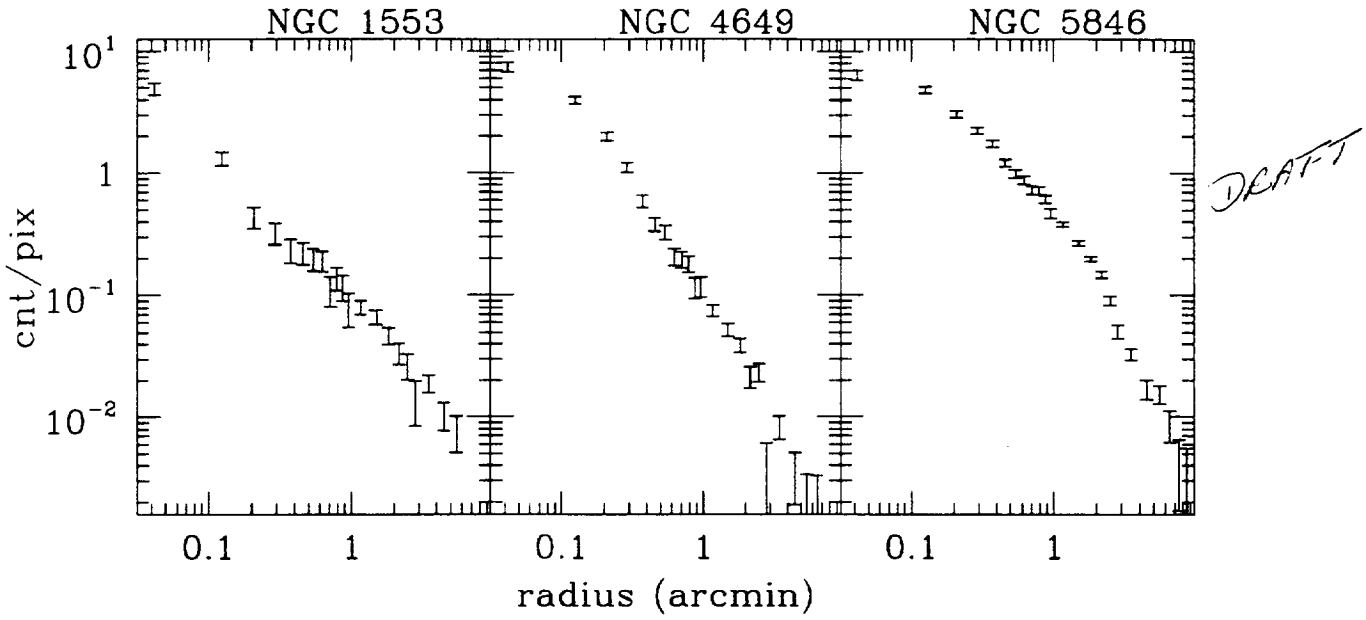

Fig. 8. Radial distribution of the net emission from the sample galaxies

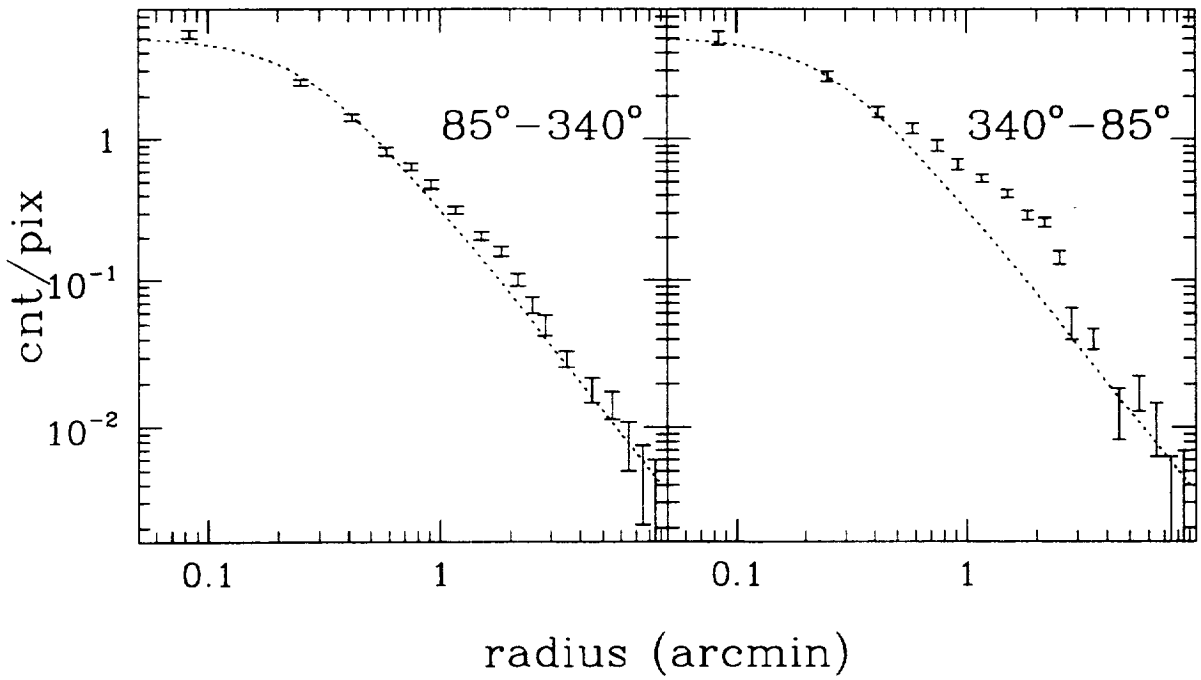

Fig. 9. Radial distribution of the net emission of NGC 5846 in different angular sectors.

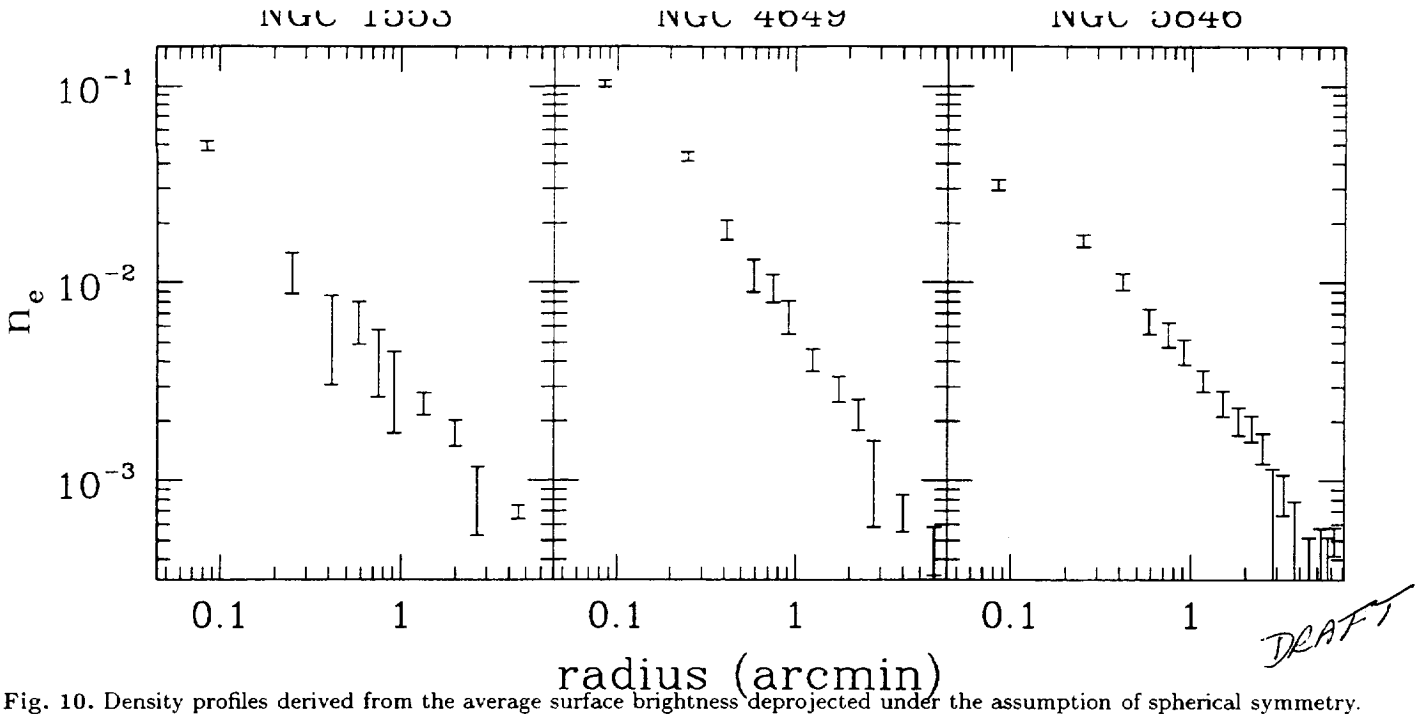

Fig. 10. Density profiles derived from the average surface brightness deprojected under the assumption of spherical symmetry.

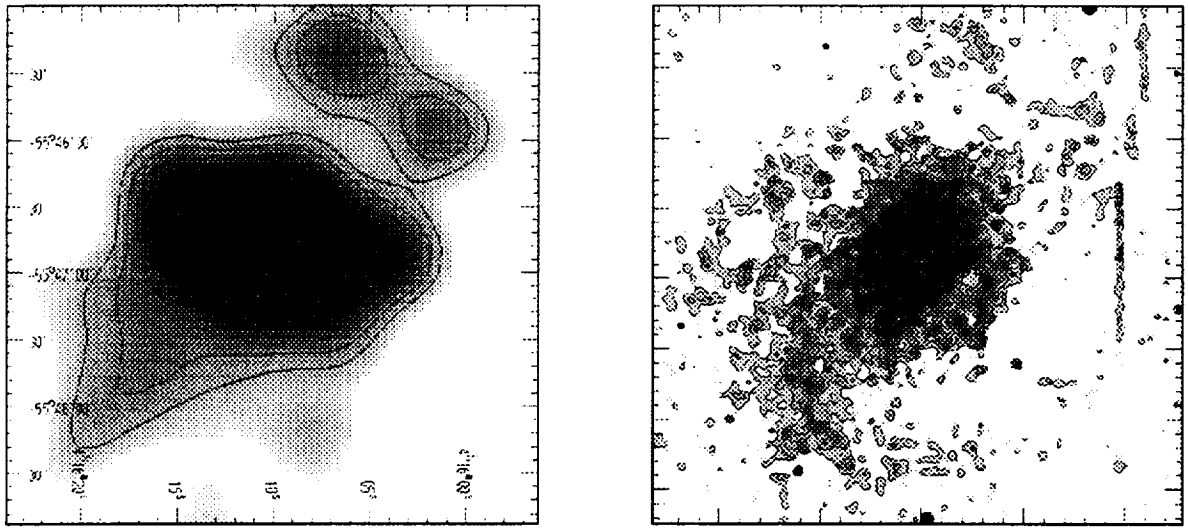

Fig. 11. Comparison between the Hα and X-ray morphologies for NGC 1553. Left: Hα data from diSerego et al 1996. The celestial coordinates of the Hα map have been assigned a posteriori without proper absolute calibration (the peak position was assigned the RC3 coordinates of the nucleus of NGC 1553). ** Check with livia ** The scale however is correct. A Gaussian smoothing with σ= 3 pixel is applied to the raw data to enhance the low surface brightness features.

Fig. 12. Comparison between the Hα and X-ray morphologies for NGC 4649. Hα data (right) are from Trinchieri & diSerego 1991. The celestial coordinates of the Hα map have been assigned a posteriori without proper absolute calibration (the peak position was assigned the RC3 coordinates of the nucleus of NGC 4649). ** Check with livia **

Your thesaurus codes are:
11(11.05.1; 11.09.04; 11.09.1)

ASTROPHYSICS
11.7.1996

ACCEPTED IN ASTRONOMY & ASTROPHYSICS

ROSAT PSPC Observations of 5 X-ray bright early type Galaxies

G. Trinchieri[1],[2], G. Fabbiano[3], and D-W. Kim[4]

[1] Osservatorio Astronomico di Brera, Via Brera 28, 20121 Milano ITALY
[2] Visiting Astronomer, Max-Planck Institut für extraterrestrische Physik, Garching bei München, Germany
[3] Harvard-Smithsonian Center for Astrophysics 60 Garden St., Cambridge, MA 02138 USA
[4] Chungnam National University, Dept. of Astron. and Space Sci., 305-764 Daejeon KOREA

Abstract. We report on the ROSAT PSPC observations of 5 X-ray bright early-type galaxies. Their X-ray morphology is more complex than *Einstein* data had shown, ranging from the ellipsoidal shape of NGC 533 to the $\sim$ 200 kpc tail of NGC 7619. Hot gas at an average temperature of 0.8-1 keV dominates their X-ray emission. The spectral analysis is based on the assumption of a hot thin plasma at solar abundances, since the spectral resolution of the PSPC does not allow unambiguous measures of the model parameters (temperatures, low energy cut-off, metal abundance). However, the estimated temperature are not strongly affected by this choice. A temperature distribution of the hot interstellar medium is also derived. Higher temperatures are in some cases observed at larger radii, while the innermost 1′ region is cooler in all of the objects studied. Due to the large range in distances however this corresponds to significantly different galaxy radii, from 5 kpc in NGC 4649 to 30 kpc in NGC 533.

The temperature and density distributions derived are used to estimate the total mass of these systems, which span from $M_T \sim 10^{12} - 10^{13}$ $M_\odot$ and corresponding mass-to-light ratios M/L $\sim$ 10-150 in solar units. Formal errors on the derived masses are estimated to be $> 25\%$.

Care must be taken in comparing results for different systems, since some of the emission attributed to these objects could suffer from the contribution for the groups and clusters they belong to. Accordingly, our mass estimates could reflect the effect of the cluster/group potential.

Key words: – Galaxies: individual: NGC 533 – Galaxies: individual: NGC 2563 – Galaxies: individual: NGC 4649 – Galaxies: individual: NGC 7619 – Galaxies: individual: NGC 7626 – Galaxies: elliptical and lenticular – Galaxies: ISM

1. Introduction

Einstein observations of early type galaxies have established that a hot interstellar medium (ISM) dominates the emission in the X-ray brightest objects. This discovery is very important for many reasons: 1) it has indicated the presence of substantial amounts of ISM in these objects; 2) it has provided a potentially powerful tool for estimating total galaxy masses at large radii; 3) it has provided a new wealth of parameters for the understanding of the enrichment of the intercluster medium. However, with *Einstein* data, we had not been able to achieve a good understanding of the detailed properties of the hot ISM. Average spectral parameters, over the entire source extent, could be estimated, albeit with large uncertainties. The morphological appearance and total extent of the hot ISM could only be roughly estimated.

The improved spatial and spectral resolution of the PSPC (Position Sensitive Proportional Counter) instrument on board the ROSAT satellite (Trümper 1983; Pfeffermann et al 1987) has proven to be crucial in furthering our understanding of the properties of the X-ray emitting gas in early type, normal, nearby galaxies. Its softer energy

Send offprint requests to: G. Trinchieri

early type galaxies (*e.g.* NGC 4636, Trinchieri et al 1994; NGC 507, Kim & Fabbiano 1995 among others). This work suggests that that the hot ISM is not isothermal over the entire source, but can show a slow temperature increase over a large region ($\sim$ 40 kpc in NGC 4636), and that its morphology is far from smooth and regular, but can show asymmetries and inhomogeneities (*e.g.* NGC 507).

In order to better understand the characteristics of the ISM in early type galaxies we have observed 5 X-ray bright early type galaxies for which *Einsetin* data had already established the presence of a dominating hot gas component in their X-ray emission. The environment in which the galaxies sit spans a large range in richness, from the low density environment of NGC 533 (in the vicinity of A193, it is at the same recessional velocity but it is located at $> 3°$, or > 6 Mpc, from the cluster center, and it is not considered as a possible member, Chapman et al 1988; it is instead one of 4 members of group GH14, Geller & Huchra 1983) to galaxies in groups and poor clusters (NGC 7619 and NGC 7626 in Pegasus I group; NGC 2563 in group A of the Cancer cluster) and galaxies in richer clusters (NGC 4649 in the Virgo cluster, at $\geq$ 1 Mpc from the cluster center).

Table 1. Log of the Observations

Field	RA Dec (J2000)	Obs. Dates Beginning End	On Time (s)
NGC 533	1:25:31.2	14/07/93	13054
	1:45:36.0	27/07/93	
NGC 2563	8:20:36.0	11/10/93	27174
	21:04:12.0	13/10/93	
		30/04/94	22873
		02/05/93	
NGC 4649	12:43:43.2	21/12/91	14301
	11:33:36.0	27/12/91	
NGC 7619/7626	23:20:31.2	30/05/92	18234
(Pegasus I)	8:12:36.0	11/06/92	

The five early type galaxies have been observed by the ROSAT PSPC as summarized in Table 1. The two observations of NGC2563 have been merged to improve on the statistical significance of the data, after checking that the single observations yielded consistent results. The data have been analyzed using primarily the PROS software available under IRAF. The details of the spatial and spectral analysis are reported in §2. Derived quantities are discussed in §3. §4-6 are devoted to the results for the Pegasus I and Cancer groups. The general results of these observations are summarized in the conclusions.

2. Data Analysis

The early type galaxies considered here all show extended emission in X-rays. Contour plots of their smoothed images in the energy band 0.14-2.0 keV are shown in Fig. 1, 8 and 9. In this energy band the expected effect of the vignetting correction is well represented by the exposure map (a model field containing information about the effective exposure moduled by the expected vignetting, see PSPC documentation for more details) provided with the data for each observed field (see also Trinchieri et al 1994, Kim & Fabbiano 1995). We can therefore use this map to flat field the data.

The raw images have been normalized to the exposure maps, and smoothed with a Gaussian function, as specified in the figure caption. Several additional sources are visible, often embedded in the X-ray emission of the target galaxy. These possible interlopers were conservatively excluded from the subsequent analysis, unless otherwise noted, by masking out circles at the source positions with radii chosen to be comparable to the outer contour (typically at 2 σ) on the contour maps. The presence of several, possibly unrelated, sources in the field is not surprising. From the LogN-LogS function derived from ROSAT data (Hasinger et al 1993) we can estimate that $\sim$ 6 sources will be present

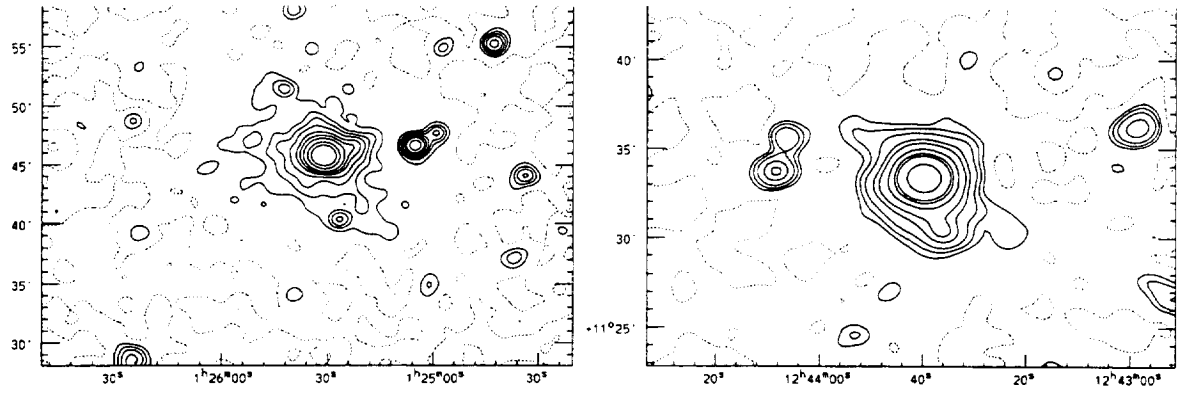

Fig. 1. Isointensity contour plots of NGC 533 and NGC 4649. Data in the 0.14-2.0 keV energy range have been normalized by the exposure map, and smoothed with a Gaussian function with $\sigma = 30''$. A constant background value has been subtracted. The dashed contour is for 0 counts. Other contours are at 2σ, 3σ, 4σ, 5σ, and higher.

in the inner ~ 0.3 square degree field at $f_x \geq 4 \times 10^{-14}$ erg cm^{-2} s^{-1}, and ~ 20 if the flux limit is lowered to 2×10^{-14} erg cm^{-2} s^{-1}.

The NGC2563, NGC4649 and NGC7626 images show extended and azimuthally symmetric emission. The external X-ray isophotes of the NGC533 map instead show a more elliptical shape. A tail of emission is observed to the SW of NGC7619, extending for about 10′ away from the X-ray peak.

2.1. Radial Count Distribution

To estimate the size of the X-ray sources associated with these galaxies, we have produced plots of the radial distribution of the X-ray emission and compared them with the expected background, estimated from the properly normalized corresponding exposure map (Fig. 2). We have used concentric annuli, centered at the source peak position, with width varying from 0.25′ to $2' - 3'$ depending on the counting statistics. The profile of the Pegasus I group is centered on NGC 7619.

Table 2. Parametric Representation of Radial Distribution of the X-ray Surface Brightness outside r$\sim$ 2′

Galaxy	R^a_{max}	α
NGC 533	16′	-1.95±0.14[b]
NGC 2563	14′	-1.18±0.07
NGC 4649	13′	-2.51±0.18
	7′	-3.39±0.25
NGC 7619	22′	-1.45±0.06[b]
		-1.28±0.17[c]
NGC 7626	3.′5	-2.87±0.05[d]

[a]Maximum radius used in the fit
[b]For the azimuthally averaged profile
[c] From 4′ to 22′, in the 250° pie region that excludes the X-ray tail
[d] From 1.5′ to 3.′5 only.

It appears that the profile of the NGC4649 field has the same shape as the exposure map from r$\sim$ 10′. However, two different normalizations are necessary to match the level of emission, one in the $\sim 10' - 16'$ annulus and a lower one outside of $\sim 25'$ (both shown in the figure). A more careful determination of the shape and level of the background will be necessary for this object; however, in this work we will consider both possibilities and will discuss the differences in the two cases.

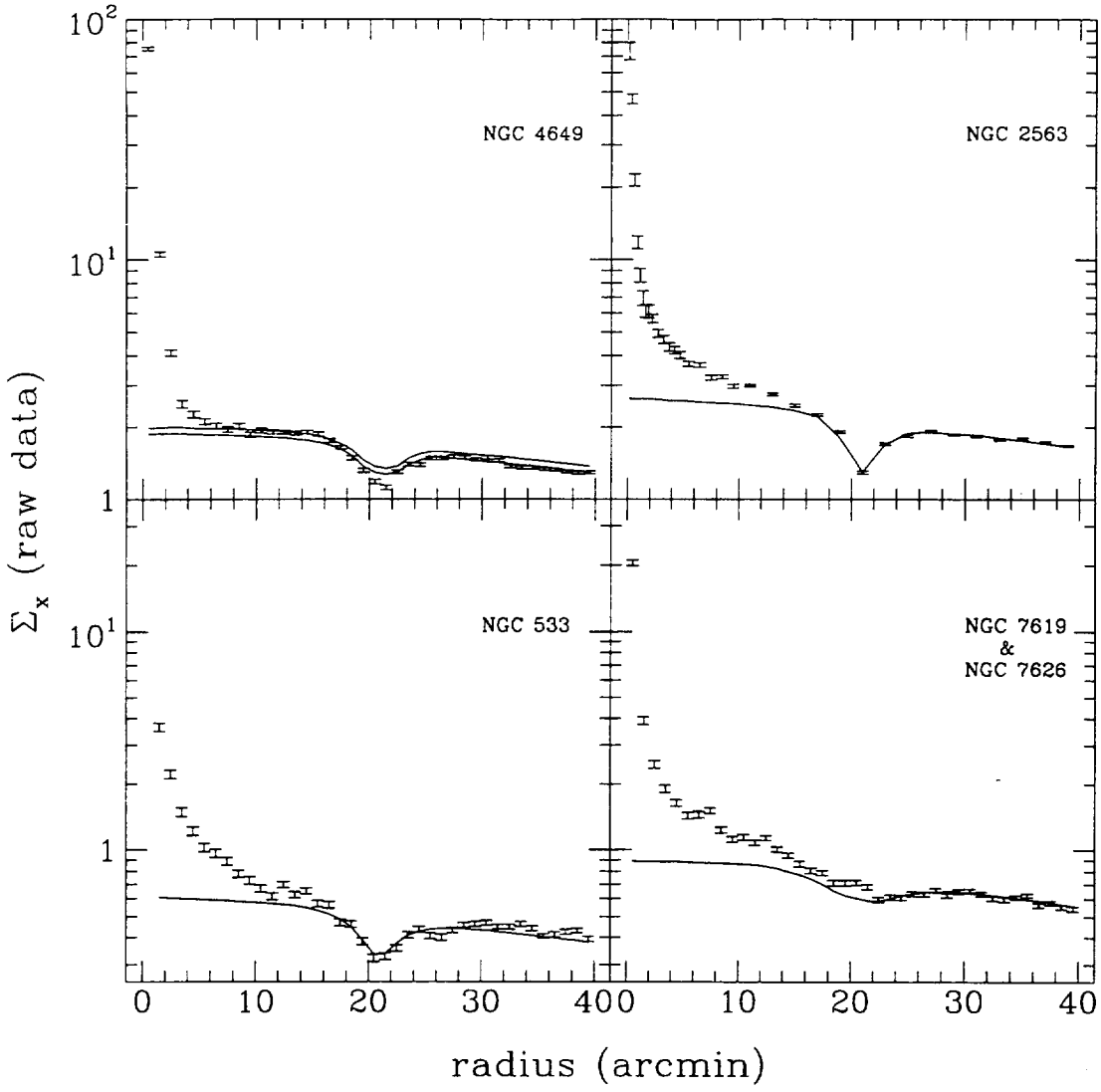

Fig. 2. Radial surface brightness distribution of the raw counts, in concentric annuli centered at the X-ray peak position (coincident with the optical position of the galaxy's nucleus). The solid line represents the background model we have assumed for each field, derived from the exposure map properly rescaled to the data. The two lines shown for NGC 4649 represent two different normalization values (see text). The profile of NGC 7619 & NGC 7626 is centered on NGC7619, offset from the field's center. Consequently, the "dip" in the exposure map profile here is not as pronounced as in the other cases.

As can be seen from Fig. 2, the exposure map represents a good fit to the emission in the region outside $\sim 20'$ from the field center (*e.g.* outside of the ring of the support structure for the PSPC that has a shape reminiscent of a "wagon wheel" and that can be recognized as a "dip" in both source data and exposure map profiles).

The net count distributions are plotted in Fig. 3 to 5 for each galaxy. Two Point Spread Functions (PSF), one appropriate for on-axis sources with temperatures of 0.2 keV (the softest PSF available with the PROS software) and one for a kT corresponding to the best fit temperature of the innermost circle (see §2.2), are also plotted for comparison, normalized at the central bin. In all cases the emission is clearly larger than either PSF, although in most cases the 0.2 keV PSF is a reasonable representation of the data for $r \leq 1'$. The spectral results however indicate significantly harder emission in that region (cf. §2.2).

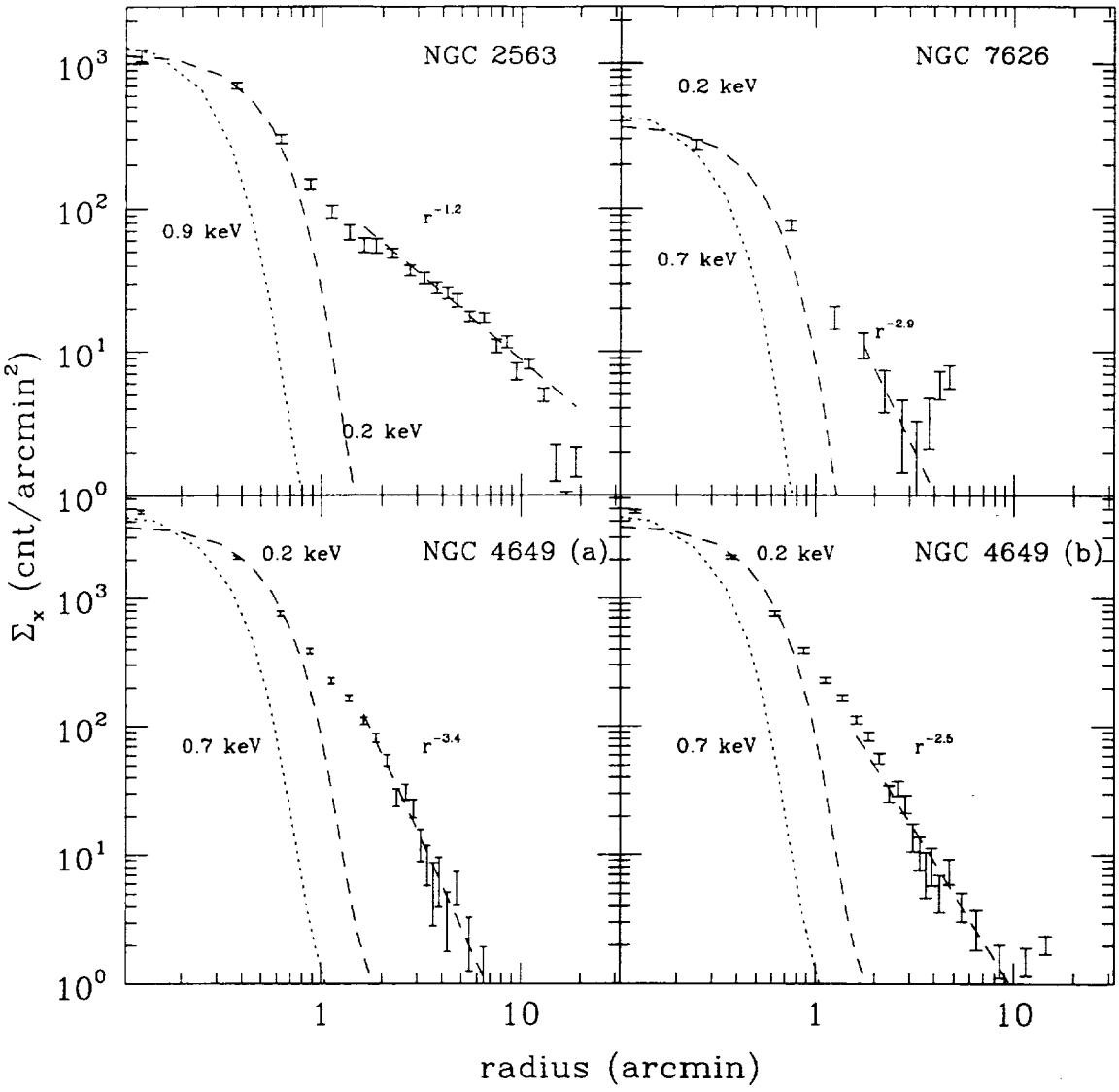

Fig. 3. Radial surface brightness profile of the net X-ray emission, in concentric circular annuli, for NGC 2563, NGC 4649 and NGC 7626. The power law fits of Tab. 2 are reported on the data.

Fig. 4 and 5 show both the azimuthally averaged profiles of NGC533 and NGC7619 and the comparison of the emissions from different pie regions. In NGC 533 there is an indication of a significant change of slope at r$\sim$ 1′. This could be interpreted as due to the presence of an unresolved, very soft core, since the emission within 1′ radius is well approximated by the 0.2 keV PSF. However, this is in contrast with the spectral results (§2.2), that indicate an average kT of 0.9 keV in the inner 1′ circle. More likely, the difference is due to the dominating contribution of the galaxy relative to the group emission (1′ $\sim$ 30 kpc at the galaxy's distance).

Fig. 4b compares the NE-SW sectors averaged together (i.e. a 70° cone along position angle PA=35°, counterclockwise from North) to that in the NW-SE ones (PA=125°). Outside of r$\sim$ 5′ – 6′, the surface brightness along PA=35° is flatter and significantly higher than that from the complementary regions.

In Fig. 5b, the region SW of NGC7619 (from 170° to 280°, corresponding to the 'tail' visible in the contour plot of Fig. 8), and the complementary region are compared. The SW profile appears significantly higher than in the other angular sector for r> 2′, although it is not a simple radial function. This is consistent with a closer inspection of the

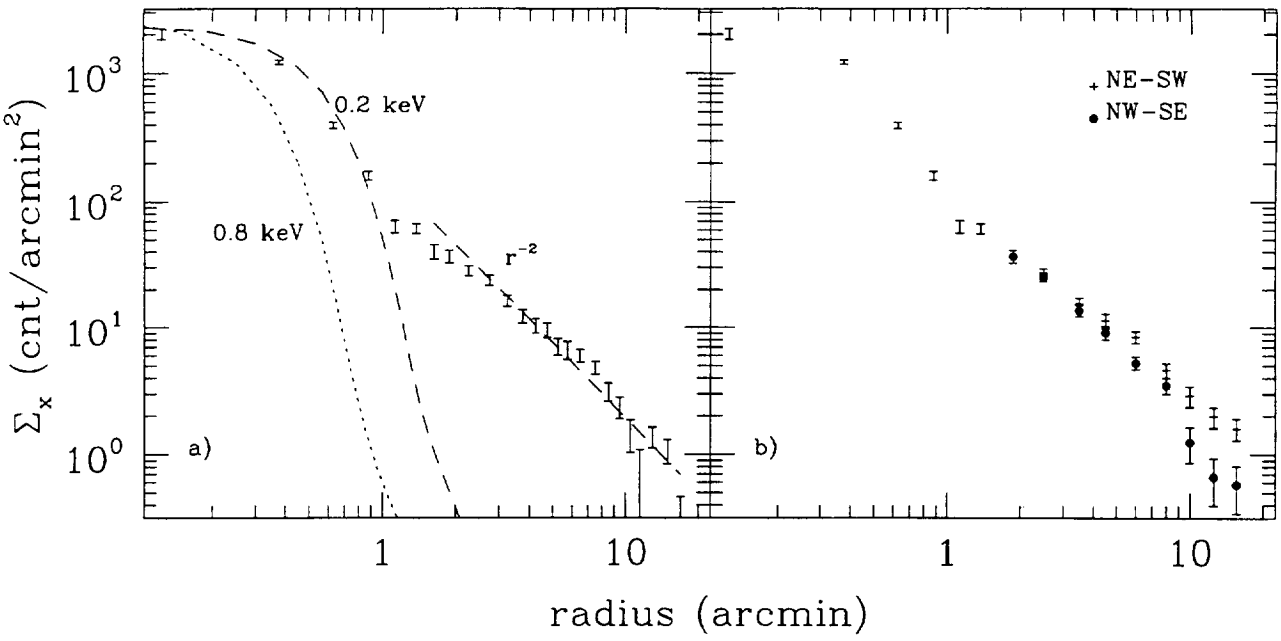

Fig. 4. Radial surface brightness profile of the net X-ray emission of NGC533, azimuthally averaged (a), and in complementary pie regions (b), as described in the text. In the inner 2′ the profile in b) is azimuthally averaged as in a).

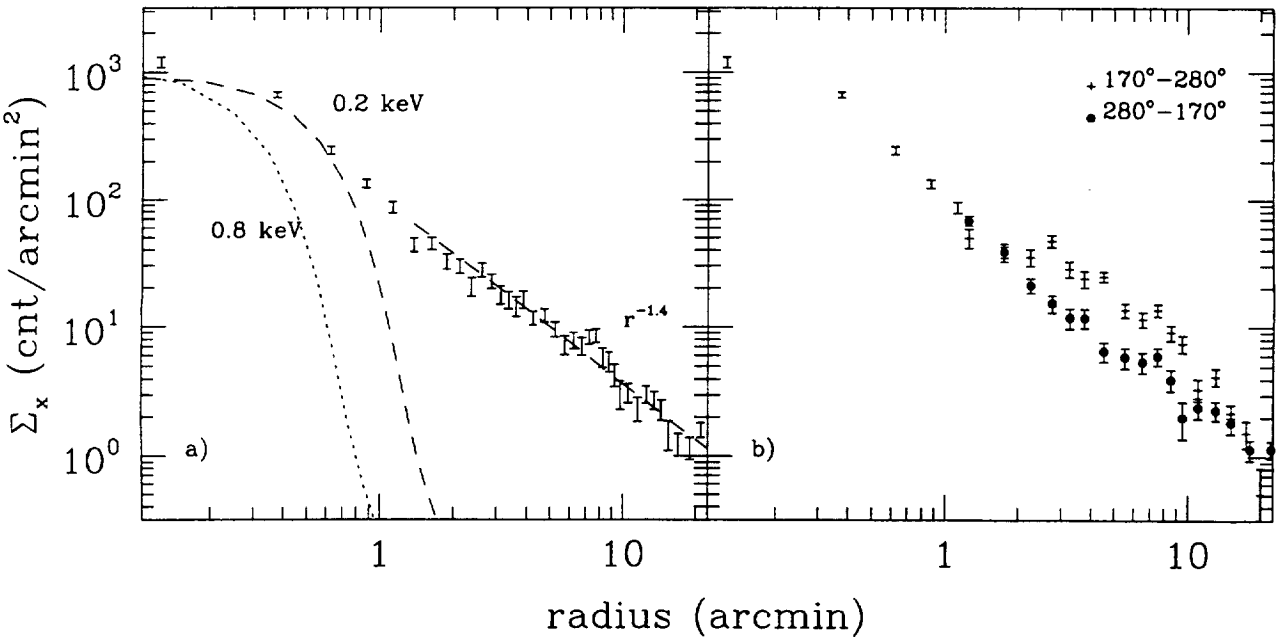

Fig. 5. Radial surface brightness profile of the net X-ray emission of NGC7619, azimuthally averaged (a), and in complementary pie regions (b). In the inner 1′ the profile in b) is azimuthally averaged as in a).

Although surface brightness profiles have traditionally been represented by a two parameter model (a core radius r_x and a radial dependence parameter β), the core radii in these galaxies are smaller than the PSF of the instrument, as suggested by the higher spatial resolution data of some of these (see for example Trinchieri et al 1986), so that determining r_x is not extremely meaningful. We have therefore fitted the radial dependence of the profile at large radii with a simple power law fit (Tab. 2). Outside of a radius of 2′ the influence of the PSF and of r_x are negligeable. There is a large variety of radial dependencies of Σ_x, spanning from the flattest distribution of NGC2563 ($\Sigma_x \propto r^{-1.2}$) to the steepest NGC 4649 ($\Sigma_x \propto r^{-3.4}$).

2.2. Spectral data

As already shown by previous studies (Trinchieri et al 1994; Buote & Canizares 1994; Fabbiano et al 1994; Bauer & Bregman 1996) the spectral capabilities of ROSAT do not allow us to measure the metallicity of the gas, since the results obtained from models of varying metallic contents are at best ambiguous. We have therefore assumed a thermal plasma model with low energy absorption and fixed the gas abundances at the cosmic value. We have however checked how much different abundances would affect the results obtained and discuss the results at the end of this section.

We have based the spectral analysis primarily on the IRAF/PROS software, which uses the same 34 channels of pulse height defined by the 'SASS' (see ROSAT Data Production Guide, by Downes, White and Reichert). To obtain the temperature in different regions, the data are extracted in concentric annuli of varying widths. The background is taken in a region considered free of emission, from the same field to ensure that its spectral distribution is the correct one for that particular observation, and is then corrected for differential vignetting before subtraction, as described in the PROS documentation. In general, the annulus at $25' - 27'$ from the field center has been used to estimate the background. Other choices made for NGC 4649 and the Pegasus field are discussed below. An average temperature, over the entire source, is also derived for completeness.

Tables 3a through 3e summarize the spectral results for each galaxy separately, graphically shown in Fig. 6. A cooler inner region, and a general tendency of increasing temperatures with galactocentric radii are seen, with the exception of NGC 2563, for which the temperature outside the inner 1′ is isothermal at $\sim$ 1.1 keV. For NGC 533 a drop in the temperature is also observed outside of a 6′ radius, although with large errors.

There is no clear trend of varying low energy absorption with radius, with the exception of the central bin of NGC 4649, where the fitted values of N_H is higher than outside. Often however N_H is not very well constrained.

Briefly for each galaxy:

NGC 533 : The average gas temperature within r $\sim$ 6′, *i.e.* before the radial profile becomes asymmetric, is $\sim$ 1 keV, in the assumption of a 1-Temperature model. This however gives a relatively high χ^2_{min} value of 42.9 for 25 degrees of freedom (DOF), that is significantly lowered ($\chi^2_{min} \sim 19.6$) by adding a second temperature in the model. The two best fit temperatures become kT_1=0.30-0.90 [at the 90% confidence limit] and $kT_2 > 1.2$ keV. The suggestion that at least 2 temperatures are present in the data is well justified by the temperature profile obtained at different radii. In fact, when the emission is divided in 3 concentric annuli, the temperature increases from 0.9 [0.85-0.95] at the center to > 1.1 keV in the outermost bin.

If the whole $\sim$ 17′ region is considered, the average temperature also is around 1 keV, however the errors become larger and the χ^2_{min} value does not require a two-temperature fit as in the case above.

NGC 2563 : The spectral distribution of the data obtained in the two observations have been compared to assure ourselves of their consistency, before merging the two data sets for the following analysis.

The average gas temperature within r=15′ is kT$\sim$ 1.06 keV, with an acceptable $\chi^2_{min} = 24$ for 23 DOF. The temperature profile obtained in 7 concentric annuli indicates a cooler core in the inner 1′ radius, and a constant $\sim$ 1.1 keV value outside, although a possible indication of a temperature decrease with radius is visible in the data (see Fig. 6).

NGC 4649 : Given the uncertainty in the normalization of the background template, we have considered both the $25' - 27'$ annulus used for all other fields, and an annulus at $11' - 13'$ for background estimates. This latter choice has the advantage that the vignetting corrections are reduced. Moreover, if the Virgo cluster is responsible for the "extra" emission outside of $\sim$ 7′, we would subtract it from the galaxy data. A comparison of the spectral distribution of the data in the two regions ($11' - 13'$ vs $25' - 27'$) however shows that they are consistent within the errors. In the present analysis we have chosen the $11' - 13'$ annulus as background.

a) NGC 533

Ann. (′)	Net counts	Chan.	kT (keV)	90% confidence region	N_H (cm^{-2})	90% confidence region	χ^2_{min}	ν	Notes
0-1	1334.4±41.6	5-28	0.904	0.84-0.94	20.41	20.25-20.55	23.5	21	
1-3	812.7±36.9	5-30	1.074	0.99-1.22	20.23	20.05-20.40	16.2	23	
3-6	897.8±46.1	5-28	1.299	>1.07	20.22	<20.45	18.9	21	
6-10	985.8±63.9	5-28	0.941	0.83-1.08	19.74	<20.20	9.6	21	
10-17	353.6±41.3	5-8	1.024	>0.80	19.60	<20.20	12.2	17	
		10-25							
0-6	3093.0±70.7	5-32	1.028	0.98-1.07	20.26	20.20-20.35	42.9	25	
			0.552	0.30-0.90	20.33		19.6	23	1
			1.228	>1.2					

b) NGC 2563

Ann. (′)	Net counts	Chan.	kT (keV)	90% confidence region	N_H (cm^{-2})	90% confidence region	χ^2_{min}	ν	Notes
0-1	1143.5±40.5	5-30	0.848	0.80-0.92	20.40	20.20-20.60	17.8	23	
1-3	1302.8±53.0	5-30	1.177	1.07-1.38	20.40	20.20-20.60	22.1	23	
3-5	1176.3±60.1	5-30	1.244	1.10-1.55	20.40	20.15-20.70	19.4	23	
5-7	1308.1±72.1	5-30	1.192	1.08-1.38	20.38	20.15-20.55	19.1	23	
7-9	1269.0±82.6	5-30	1.025	0.91-1.15	20.22	<20.70	20.7	23	
9-12	1867.4±116.6	5-10	1.075	0.97-1.27	20.00	<20.35	17.5	21	
		13-30							
12-15	1149.6±127.7	5-10	1.014	0.83-1.35	19.60	<20.60	15.3	17	
		13-26							
0-15	9050.1±312.0	5-30	1.058	1.01-1.14	20.20	20.00-20.40	23.9	23	

c) NGC 4649

Ann. (′)	Net counts	Chan.	kT (keV)	90% confidence region	N_H (cm^{-2})	90% confidence region	χ^2_{min}	ν	Notes
0-1	3670.0±66.1	5-30	0.814	0.78-0.83	20.28	20.25-20.35	27.2	23	
			0.756	0.46-0.80	20.36	—	14.1	21	1
			2.91	>1					
1-2	1237.2±44.0	5-28	0.898	0.83-0.96	19.99	19.75-20.20	15.3	21	
2-3	463.8±34.8	5-7,9-29	0.923	0.78-1.08	19.74	<20.25	14.0	21	
3-6	388.7±61.7	6-9,11,12	1.315	>0.93	19.60	< 20.60	15.8	16	
		14-26							
0-6	5741.2±112.9	5-32	0.853	0.82-0.90	20.10	19.95-20.30	47.9	25	
			0.793	0.64-0.84	20.20	—	30.5	23	1
			3.000	> 1.2					

d) NGC 7619

Ann. (′)	Net counts	Chan.	kT (keV)	90% confidence region	N_H (cm^{-2})	90% confidence region	χ^2_{min}	ν	Notes
0-1	972.4±36.8	5-30	0.775	0.70-0.82	20.59	20.40-20.85	12	23	
1-3	858.3±39.6	5-29	0.885	0.82-0.94	20.55	>20.25	17.6	22	
3-10	1073.6±49.1	6,7,9-30	0.948	0.88-1.02	20.41	20.10-21.10	19.2	21	2
0-10	2886.4±72.6	5-29	0.880	0.84-0.92	20.58	20.40-20.85	27.8	22	2
			0.812	0.60-0.88	20.67	—	19.5	20	1
			3.00	> 1.1					
"group"	2150.1±143.6	5-7,9	1.267	1.10-1.90	20.04	19.50-20.40	13.3	20	
		11-29	3						

ej NGC 7626

Ann. (′)	Net counts	Chan.	kT (keV)	90% confidence region	N_H (cm^{-2})	90% confidence region	χ^2_{min}	ν	Notes
0-1	404.4±26.1	6-30	0.737	0.58-0.88	20.48	>20.20	18.9	22	
0-3	613.5±34.1	8-28	0.826	0.68-0.90	20.50		25.2	18	

Notes to the Table:
The line-of-sight N_H value is: ~ 20.5 for NGC 533;~ 20.7 for NGC 2563, NGC 7619 and NGC 7626;~ 20.4 for NGC 4649 (Stark et al 1992).

1 A two temperature fit is used. kT_1 and kT_2 are given on successive lines. The errors are derived for kT only
2 Limited to the 170°-280° sector in the 3′ – 10′ annulus.
3 "group" is the region from 2′ to 16′, centered on NGC 7619, and excluding the 170°-280° sector.

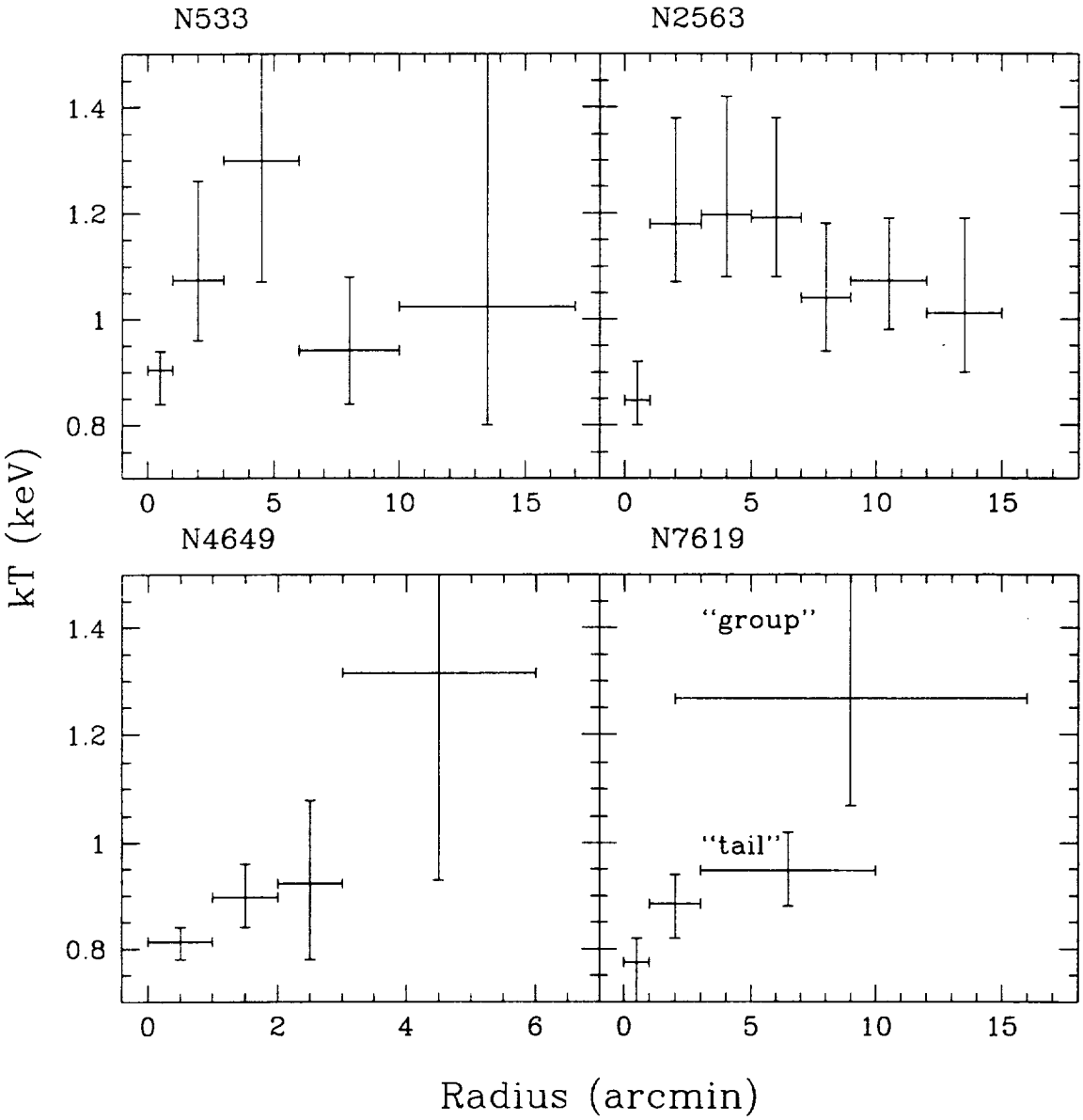

Fig. 6. Summary Plot of the Temperature Parameters Derived for Different Annular Regions in the Sample Galaxies.

0.84 keV, and $kT_2 > 1.2$ keV at the 90% confidence level. No further reduction of χ^2_{min} is achieved with the addition of a third component.

A slow increase of T towards large radii, and a higher value of the absorbing column in the innermost 1′ circle are suggested by the data.

Pegasus I group : The contour map and the radial profile show that the emission from the Pegasus I group field covers the inner 20′ circle, and it is likely to extend further out, with the possible exception of a region north of the NGC7619 galaxy. We have therefore tried both this region of low emission and the annulus at $25' - 27'$ for background estimates. The former choice would have the advantage of smaller corrections, but with a larger statistical uncertainty due to the smaller area covered. As for the case of NGC4649 however, a comparison between the spectral distribution of the data in the two regions shows consistency within the statistical errors. We have therefore used the outer annulus as background in the following analysis.

The source associated with NGC7619 has been divided into two annuli within r=3′, and the "tail", in the SW quadrant, from $3' - 10'$. Tab. 3d indicates that there is a significantly cooler 1′ core, and that the tail is harder than the galaxy. The group gas (in the $2' - 16'$ region, excluding the "tail") is also harder than the tail. The low energy absorption is not well constrained, and is in general consistent with the line of sight value.

NGC7626 extends only out to r∼3′, and the total number of counts detected does not allow us to examine the spectral distribution of the data in different regions. The average temperature over the whole 3′ circle is kT∼0.83 keV with a χ^2_{min} of 25.2, which is entirely consistent with the temperature obtained from just the innermost 1′ circle.

We have also examined the spectral distribution of the data of the galaxies above the possible cluster emission by assuming as background the annulus at $4' - 10'$ from the field center, with the exclusion of a 3′ circle at the position of the two galaxies. The resulting best fit parameters are consistent with those reported in Table 3.

Metal Abundance In order to explore the effect of different abundance models on the temperatures derived, we have redone the spectral fits for a few of the cases presented in Table 3, where the statistics is higher, fixing the abundance parameter at 20% the cosmic value.

The absolute values of the temperatures are smaller (< 0.1 keV in all cases examined, and typically is $\sim 0.05 - 0.06$) and the low energy cutoff values are higher (typically, ~ 0.3 in log N_H) in the case of 20% abundances, but the trends and the uncertainties on T are preserved. The values of χ^2_{min} are also consistent with one notable exception, given by the global spectrum of NGC533 (in the $0' - 6'$ annulus). The 20% abundance model gives an acceptable χ^2_{min}=24 for kT=0.95 and N_H=20.6 (χ^2_{min}= 43 for the 1-temperature model at 100% cosmic abundance, Tab. 3). To obtain a similar χ^2_{min}, a 2 temperature model must be assumed for 100% cosmic abundances. This is however an indication of the ambiguity with which the spectral parameters can be derived from the limited spectral resolution of the ROSAT PSPC (cf. Figure 7 in Trinchieri et al. 1994).

3. Derived quantities

3.1. Fluxes and Luminosities

Table 4 summarizes the resulting fluxes and luminosities for the sample galaxies within the given radius R_m. The counts to flux conversion is derived from the parameters of the best fit spectral model of the source as a whole. However, the fluxes are entirely consistent with those obtained by summing the contribution of each annulus, accounting for the different spectral parameters obtained for each of them.

Luminosities are in the range $L_x \sim 2 - 60 \times 10^{41}$ erg s^{-1}, at the top of the distribution of X-ray luminosities of early type galaxies (see Fabbiano et al 1992).

3.2. Density profiles

The radial profiles, together with the spectral results, have been used to derive the radial dependence of intrinsic gas parameters: electron density, cooling time and total gas mass. Since the observed surface brightness profile is the integral along the line of sight, a deprojection of the observed quantity is needed to obtain the intrinsic distribution (Kriss et al 1993). However, the temperature of the gas must be known to derive its density, and the preceding analysis

Galaxy	R_m^a ′ (kpc)	Counts[a]	Flux[b] erg cm^{-2} s^{-1}	L_x^b erg s^{-1}	D Mpc
NGC 533	18(565)	4321±115	4.19×10^{-12}	5.90×10^{42}	108
NGC 2563	20(560)	8612±220	2.28×10^{-12}	2.53×10^{42}	96
NGC 4649[c]	7(35)	5890±103	4.62×10^{-12}	1.61×10^{41}	17
NGC 4649[d]	17(84)	7418±197	5.82×10^{-12}	2.02×10^{41}	17
NGC 7619[e]	10(225)	2980±60	2.23×10^{-12}	1.51×10^{42}	75
NGC 7626	3.5(75)	623±34	4.21×10^{-13}	2.83×10^{41}	75

[a] The maximum radius R_m (in ′ and in kpc in parenthesis) and the counts given are consistent with the radial profiles of fig. 3-5 in the energy range 0.14-2.00 keV.
[b] Single temperature fits have been used for all galaxies
[c] The background template is normalized to the data in the $11' - 13'$ annulus
[d] The background template is normalized to the data in the $25' - 27'$ annulus
[e] Azimuthally averaged for $r \leq 3'$, and in the 170°-280°sector for $3' < r \leq 10'$

has only provided us with the projected values. A proper deconvolution of the spatial/spectral data is needed to derive this quantity. We have however approximated this procedure with the following assumptions: 1) the gas is assumed homogeneous, *i.e.* the gas has only one temperature at any given radius; 2) the temperature is constant in any given annulus; 3) the observed projected value of the temperature is not significantly different from the de-projected intrinsic value. This last assumption is supported by the results of the procedure used in the analysis of NGC4636 data. There Trinchieri et al (1994) had applied the same de-projection used to derive the intrinsic surface brightness distribution to the spectral data as well, and have derived the best fit parameters and errors based on the de-projected distribution. As can be seen from the comparison of their tables 1, 2 and 5, the temperatures are consistent, within the errors. Moreover, it should be remembered that the density depends weakly on the temperature, therefore small changes in kT should not affect the results significantly. Finally, while assumption 1) is probably strictly incorrect, as the temperature is in most cases an increasing function of the radius, the increase is small and the data quality is such that this approximation should not be a serious source of error. Moreover, no correction for the effect of vignetting at large radii is applied (however the error introduced by this should be small).

*The case of NGC*4649: The density profile has been derived in the assumption that the emission outside of 7′ should be considered background emission relative to the galaxy. This assumption is justified by its shape (see §2) and also by the fact that the galaxy is located in the Virgo cluster, relatively close to M87 (< 1 Mpc, for d=17 Mpc) where the cluster emission is still relatively strong (Boehringer et al 1994). The radial distribution of the net emission shown in Fig. 3 (panel b) also indicates that the profile flattens quite significantly outside of 7′, when the background is taken far from the galaxy. This could be justified again by the presence of a low surface brightness emission such as that of a cluster gas.

*The tail of NGC*7619: An asymmetric feature is present to the SW of NGC7619. Even though the asymmetry is already present at a radius r∼ 2′, we have derived the density profile within a radius of 4′ assuming azimuthal symmetry. This radius is estimated from the radial profile of the region complementary to the tail, and corresponds to a possible flattening of the profile.

The density profiles are shown in Fig. 7. Their parameterization is given in Table 5. Central densities span a relatively large range of value, 5-15 $\times10^{-3}$ cm $^{-3}$ [Note that these are probably underestimated due to the influence of the PSF which has not been removed]. This spread however could be due to the different distances of the objects, such that the inner 0.′5 circle in which the central densities are estimated refer to circles of radii 2.5 kpc, in NGC4649, and of 10 to 15 kpc for the others. Similarly, the outermost radii at which the densities are derived refer to significantly different physical sizes, from 35 kpc (NGC4649), to 90 kpc (NGC7619), to $\geq$ 500 kpc for the other galaxies.

Total gas masses and cooling times have also been derived, for a filling factor $f = 1$. Central cooling times range from $\sim 6 \times10^8$ yr for NGC 7619 to $\sim 3 \times10^9$ yr for NGC 533. At the outermost radius considered they are $< 10^{11}$ yr for NGC 4649, NGC 7619 and NGC 7626, and $\sim$ 2-3 $\times10^{11}$ yr for NGC 533 and NGC 2563. Total gas masses (listed in Tab. 5) again span a large range from $M_{gas} \sim 4\times 10^9$ to $\sim 10^{12}$ $M_\odot$. At similar physical sizes (35 kpc), M_{gas} are $\leq 10^{10}$ $M_\odot$ for all except NGC4649, which appears to contain less gas than the other objects ($\sim$ 1/2).

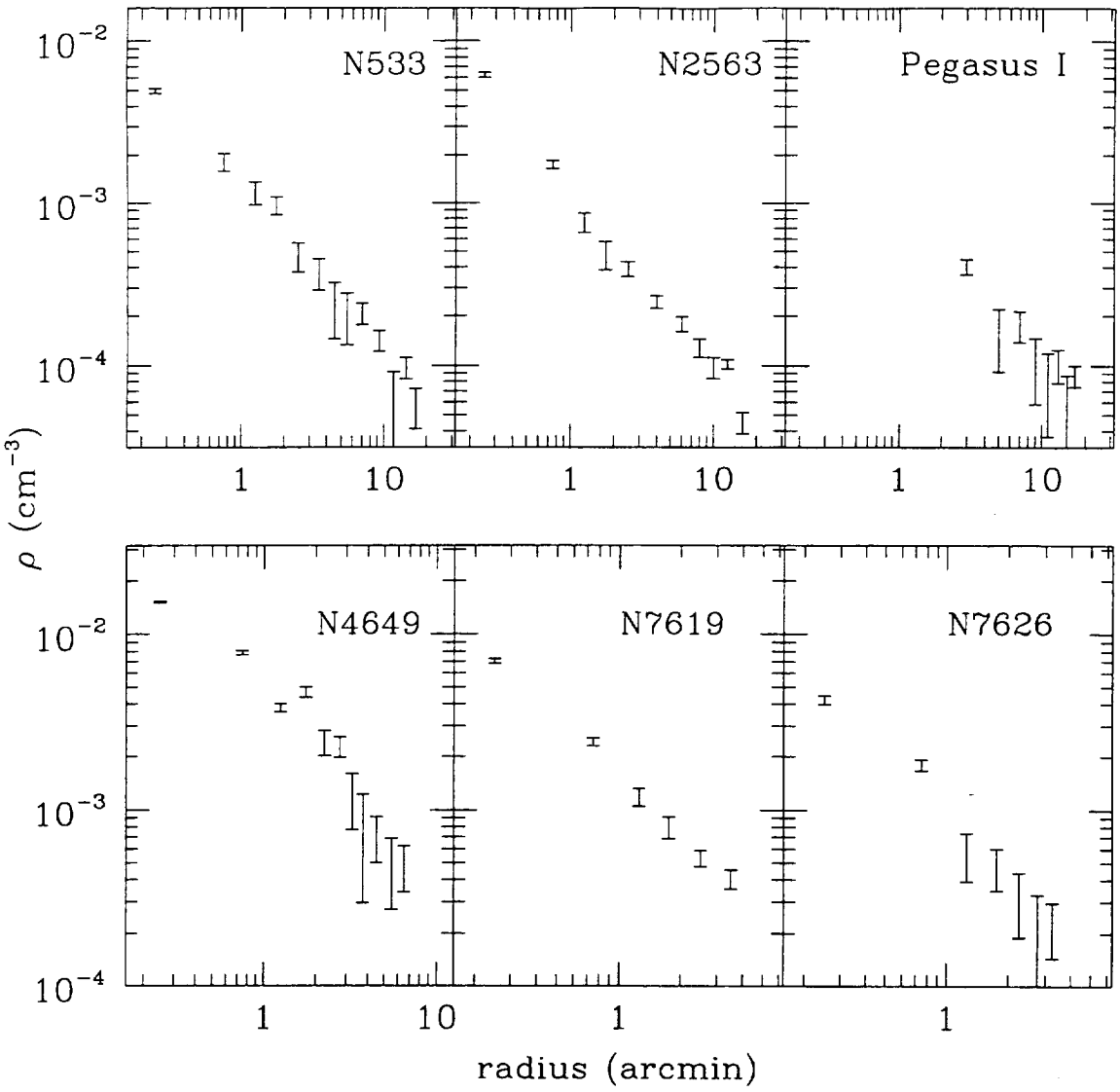

Fig. 7. Radial density distribution for the sample galaxies. The plot for Pegasus I refers to the intergalactic emission outside the "tail" feature of NGC7619 and outside the two bright galaxies NGC7619 and NGC7626.

3.3. Total Mass Determination

The temperature and density distributions can be used to estimate the total gravitational mass M_T, if the gas is assumed in hydrostatic equilibrium in the galaxy's spherically symmetric potential (Fabricant & Gorenstein 1983).

Table 5 summarizes the mass estimates for the galaxies in the present sample. These have been calculated within the maximum radii also listed in the table, using the results on temperatures and densities reported above and also listed in the table. However there are still several caveats associated with these estimates, which also prevent a reliable estimate of the errors on these quantities: a) the calculations are based on assumptions that are not exactly met (*e.g.* spherical symmetry); b) in most cases only a lower limit to the temperature could be derived at R_{max}; c) the uncertainty in the value of the temperature due to the assumption of cosmic abundances is not taken into account; d) the assumed R_{max} often does not reflect the maximum extent of the source, but it is for example the farthermost region at which the gas temperature could be determined; e) the linear fits to calculate temperature and density gradients are done using the actual values of the quantities, without taking into account their error; moreover, density

Table 5: Total Mass, Gas Mass, Mass to Light ratio and "visible"-to-total mass fraction.

Name	R_m^a '(kpc)	$\Delta\rho^b$	ΔT^c	$T(R_m)^d$ keV	M_{gas} $M_\odot$	$M_T{}^e$ $M_\odot$	M/L^f $M_\odot/L_\odot$	f^g %
NGC533	6(190)	-0.96±0.14	0.16±0.03	1.3	7.3×10^{10}	$7.3[\pm1.3]\times10^{12}$	50	20
NGC533	18(570)	-1.05±0.13	0	1.0	2.2×10^{12}	$2.2[\pm0.3]\times10^{13}$	70-160	20-15
NGC2563	15(420)	-0.81±0.06	0	1.1 ±0.15	1.3×10^{12}	$1.4[\pm0.2]\times10^{13}$	10-150	95-15
NGC4649	7(35)	-1.72±0.31	0.19±0.08	1.3	4.2×10^{9}	$2.6[\pm0.5]\times10^{12}$	50	16
NGC7619	4(90)	-0.96±0.20	0.10	0.89±0.05	4.7×10^{10}	$2.9[\pm0.6]\times10^{12}$	30	25
NGC7626	3.5(75)	-1.55±0.34	0	0.83±0.07	1.8×10^{10}	$3.6[\pm0.8]\times10^{12}$	40	20
Pegasus I	16(350)	-0.64±0.20	0	1.28±0.15	$\sim8\times10^{11}$	$1.1[\pm0.4]\times10^{13}$	60	20

Notes:

[a] Maximum radius (in ′ and in kpc in parenthesis) at which the total mass M_T is calculated

[b] Density gradients. The slope of the density profile is calculated assumning a simple power law outside of r=2′ to avoid the influence of the PSF except for NGC 7619 and NGC 7626, for which r_{in}=1′.5

[c] Temperature gradients, calculated assuming a simple power law fit. They are based on 3 points for NGC 533, on 4 points for NGC 4649 and on 2 points only for NGC 7626, for which no error on the fitted gradient is given.

[d] Temperatures at R_m. The errors are at the 68% confidence. For NGC2563, the value is an estimate of the average temperature from the results of Table 3. For NGC533 and NGC4649 no errors are given, since only a lower limit could be determined.

[e] Total mass within R_m. Proper error estimates could not be done and the errors quoted are probably underestimates (see text). They should be taken with caution.

[f] Mass to light ratios. For NGC 533 and NGC 2563 they have been estimated based on both the group (Bothun et al 1983, Geller and Huchra 1983) and on the galaxy only luminous mass, respectively.

[g] "Visible" to total mass fraction. For NGC 533 and NGC 2563 it is estimated based on both the group (Bothun et al 1983, Geller and Huchra 1983) and on the galaxy only optical luminosity, respectively.

gradients are derived assuming a power law fit to parametrize the data, which does not take into account possible effects of the PSF and r_x (although at large radii these should be negligeable) and does not take into account the effect of the energy dependent vignetting at large off-axis angles. The formal errors on M_T listed in Table 5 are therefore an underestimate of the real errors associated with the data, since some of the uncertainties have not been taken into account. The uncertainty in determining M_T can therefore be estimated to be $> 25\%$.

For NGC 533 we give two different estimates, within a radius of 6′, within which we detect a temperature gradient, and within the maximum extent of this galaxy of 18′. This latter is calculated assuming isothermality. For the Pegasus I cluster we give two different estimates of M_T, one for the individual galaxies, within a radius of 4′ for NGC 7619 and 3.′5 for NGC 7626, and one for the cluster, based on the density distribution derived in the 250° azimuthal region that avoids the X-ray tail (cf. Fig. 5).

Total masses span from $\sim 3\times10^{12}$ $M_\odot$ to $\sim 2\times10^{13}$ $M_\odot$. This large range of values once again reflects the much different scales of the X-ray emission, relative to the galaxy only (R$\sim$ 35 kpc, NGC4649) or to the group (R$\sim$ 400 kpc, NGC 2563).

Mass-to-light ratios (M/L) and the "visible" (*i.e.* stars, hot gas) to total mass fraction f have been calculated and are also given in Table 5. M/L values span from $\sim$ 20 for the NGC2563 group to 30-50 for individual galaxies to $>$ 100 for NGC533. f is of the order of $\sim$ 20% for all systems, with the exception of Cancer, for which it could be as high as $\sim$ 100%.

4. The Pegasus I Group

Fig. 8 shows the detailed X-ray emission from the Pegasus I group, superposed onto the optical plate of the area, from the "Digitized Sky Survey"[1]. The X-ray map shows that there is extended, low surface brightness emission in the area surrounding the two bright galaxies NGC 7619 and NGC 7626, that the emission is structured and that many clumps

[1] Based on photographic data of the National Geographic Society - Palomar Observatory Sky Survey (NGS-POSS) obtained using the Oschin Telescope on the Palomar Mountain. The NGS-POSS was funded by a grant from the National Geographic Society to the California Institute of Technology. The plates were processed into the present compressed digital form with their

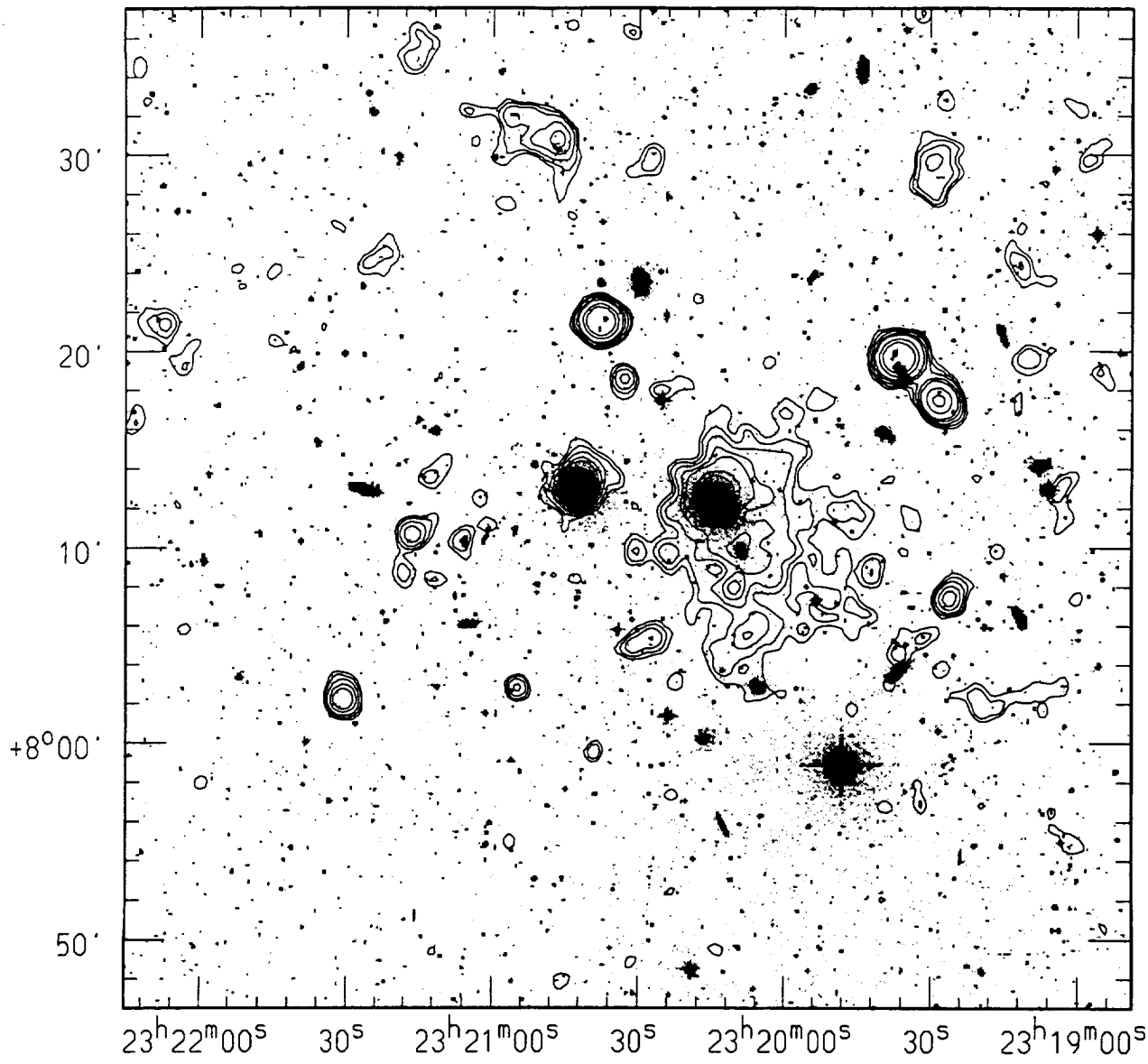

Fig. 8. Isointensity X-ray map of the Pegasus I group superposed onto the optical plate form the Digitized Sky Survey, smoothed with a gaussian function with $\sigma = 22''.5$.

or other sources are present. Table 6 lists the counts rates for the clumps present. Counts are extracted in a circle of radius given in the table and the background is estimated locally from adjacent annuli. The positions are obtained from a combination of sources found by the detect algorithm and "eye-judgment" of the contour map. The luminosity of these "clumps" is in the range 1-10 $\times 10^{40}$ erg s^{-1}, if they are at the Pegasus distance (75 Mpc).

Some of the X-ray structure is probably due to unrelated sources, most of which are coincident with optical candidates. It is clear from the map that most of the galaxies have no X-ray counterpart and vice versa, most of the X-ray sources or clumps of gas visible in the field are not associated with galaxies. The only notable exception,

permission. The Digitized Sky Survey was produced at the Space Telescope Science Institute under US Government grant NAG W-2166.

Table 6. Sources in the Pegasus I field

Source	RA	δ	Radius	Counts	Err.	f_x
	J2000		$'$			erg cm^{-2} s^{-1}
1	23:19:26.2	8:07:25.2	0.83	76.34	11.6	3.9×10^{-14}
2	23:19:28.6	8:17:20.2	0.83	275.24	19.1	1.6×10^{-13}
3	23:19:37.0	8:19:31.1	1	724.14	29.9	3.2×10^{-13}
4	23:20:09.2	8:09:57.0	0.7	25.70	11.4	1.7×10^{-14}
5	23:20:11.0	8:07:54.1	0.67	42.96	11.0	1.8×10^{-14}
6	23:20:32.9	8:18:30.5	0.83	37.66	10.2	1.6×10^{-14}
7	23:20:38.0	8:21:25.5	1	693.25	28.6	2.4×10^{-13}
8	23:20:46.5	8:30:54.2	1	78.17	13.4	4.7×10^{-14}
9	23:20:55.1	8:02:45.5	0.67	43.16	9.0	2.7×10^{-14}
10	23:21:16.7	8:10:30.3	0.83	51.30	10.7	2.4×10^{-14}
11	23:21:31.5	8:02:05.2	0.83	76.49	11.1	4.2×10^{-14}

besides the two galaxies NGC7619 and NGC7626 already discussed, is NGC 7617, an S0 galaxy of $m_B = 14.8$, clearly coincident with a peak of emission in the tail of NGC 7619. The excess counts for this source (# 4 in Table 6) are estimated on a $0.7'$ circle at the position of the galaxy, above the local background, estimated in an annulus of $0.7' - 2'$ inner and outer radii respectively concentric to the source region. If the excess is attributed to the galaxy, NGC7617 would have an X-ray luminosity of 1.3×10^{40} for a 1 keV thermal spectrum (appropriate for an early type galaxy) and line-of-sight column density. The X-ray-to-optical flux ratio of 30.1 would put this galaxy among the low X-ray luminosity galaxies, *i.e.* those galaxies in which the gaseous component does not dominate the emission (if it is present at all, see Fabbiano et al 1992).

The correspondence with NGC 7617 could alternatively be interpreted as chance coincidence, and this X-ray enhancement, together with the irregular appearance of the tail morphology, as inhomogeneities in the tail of NGC 7619. Similar inhomogeneities have already been reported in the emission of NGC507 (Kim & Fabbiano 1995), A85 and A496 (Prestwich et al 1995) and NGC1399 (Kim et al 1995) among others. A spectral analysis of such features in other groups indicates that they might be cooler denser condensations in the hot gas. Unfortunately, given the limited statistics of this observation, we can only measure the global spectral characteristics of the tail in the Pegasus I group. Cooler condensations could be the signature of density inhomogeneities induced by thermal instabilities, possibly triggered by dynamical effects. The evidence of a tail-type emission in NGC7619 would also point to dynamical effects, like stripping of gas as the galaxy moves into the denser cluster medium (the first example of a similar feature observed in NGC4406 was in fact interpreted as the result of the dynamical interaction with cluster gas, Forman et al 1979).

An intergalactic medium is known to be present from *Einstein* observations of this region (Canizares et al 1986), and it is also visible in the contour map of Fig. 8 and in the radial profile of Fig 5 out to a radius of $\sim 16' - 20'$ from the galaxy's center (the background template has been normalized outside of this region, therefore no excess can be measured at larger radii, see Section 2.1). To avoid the obscuration due to the PSPC support structure, we have however restricted our estimate of the diffuse group emission to r $\sim 16'$. In the region comprised between $2'$ and $16'$ centered on NGC 7619 and excluding the sector containing the tail (170°-280°), a $2'$ circle around NGC 7626, and the other possible interlopers, we find about 2000 excess counts. If we correct for the area excluded, we estimate a total of ~ 3200 counts in the full $16'$ circle. The spectrum of this emission is consistent with a thermal model with kT=1.1-1.9 kT (90% confidence). The flux, $f_x \sim 2.5 \times 10^{-12}$ erg cm^{-2} s^{-1}, corresponds to $L_x = 1.7 \times 10^{42}$ erg s^{-1} (D = 75 Mpc), comparable to the luminosity of the NGC7619 complex emission.

To estimate the density of the intergalactic gas, the tridimensional spatial distribution must be known. Assuming spherical symmetry, and filling factor of unity, we have derived an average density of $\sim 1.9 \times 10^{-4}$ cm^{-3}. This is probably an underestimate of the real gas density in the group since the emission does not seem to fill uniformly the observed surface (a circle of r=16$'$). The corresponding total mass of gas in the same volume is $M_{gas} \sim 8 \times 10^{11}$ $M_\odot$.

These results are entirely consistent with the estimates based on the *Einstein* data (Canizares et al 1986), and with those summarized for a sample of poor clusters of galaxies by Price et al (1991), also based on *Einstein* data.

"Digitizes Sky Survey". The total number of sources detected moreover is entirely consistent with the expected number from the LogN-LogS function of Hasinger et al (1993).

5. NGC 2563 – The Cancer Subgroup A

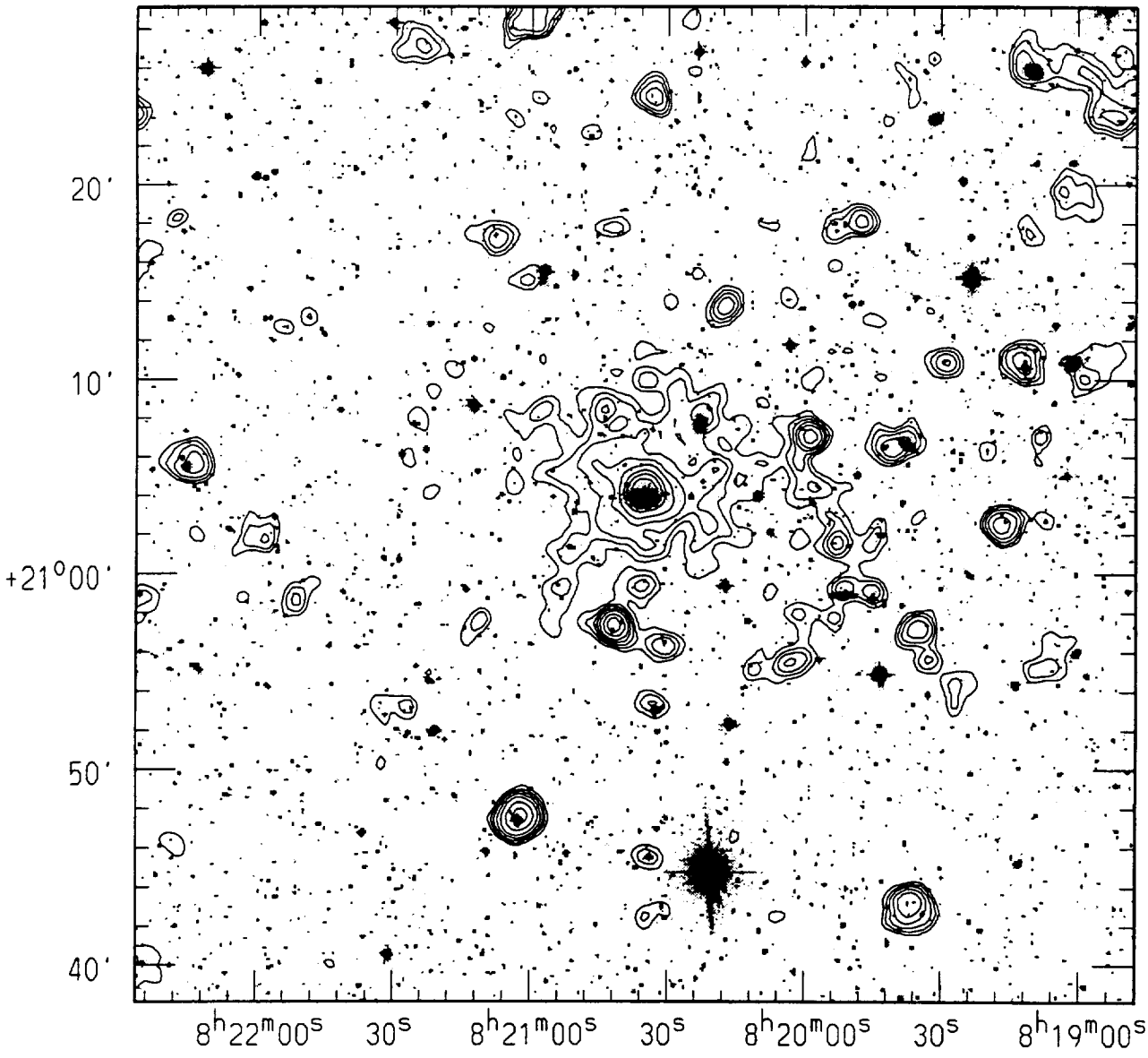

Fig. 9. Isointensity X-ray map of the Cancer subgroup A (NGC2563) superposed onto the optical plate form the Digitized Sky Survey. A smoothing function with $\sigma = 22.''5$ is applied to the data.

X-ray contours over the "Digitized Sky Survey" plate of the area), there are secondary peaks of emission, several of which, unlike in the case of the Pegasus I group, coincide with galaxies. The net counts associated to these peaks are listed in Table 7.

Table 7. Sources in the NGC 2563 field

Source	RA	δ	Radius	Counts	Err.	f_x
	J2000		$'$			erg cm^{-2} s^{-1}
1	8:18:38.5	20:46:43.7	1.5	92.34	28.79	3.80×10^{-14}
2	8:18:40.3	21:02:16.6	1.5	325.00	34.78	1.22×10^{-13}
3	8:18:52.6	21:23:25.3	1.5	155.03	29.54	6.15×10^{-14}
4	8:18:58.7	21:26:03.8	0.7	79.68	30.35	3.20×10^{-14}
5	8:19:13.2	21:10:50.7	0.7	52.29	11.22	1.78×10^{-14}
6	8:19:17.9	21:02:32.1	1.5	92.52	14.44	3.09×10^{-14}
7	8:19:28.9	21:10:49.5	1.5	129.16	28.40	4.22×10^{-14}
8	8:19:34.6	20:57:09.8	0.7	77.80	14.37	2.53×10^{-14}
9	8:19:37.1	20:42:58.9	1.5	296.93	31.58	1.09×10^{-13}
10	8:19:40.2	21:06:26.3	0.7	71.11	14.06	2.23×10^{-14}
11	8:19:47.1	21:18:13.5	0.7	61.85	12.42	2.05×10^{-14}
12	8:19:52.0	20:59:11.1	0.7	54.04	12.94	1.75×10^{-14}
13	8:19:52.9	21:01:32.3	0.7	54.04	13.17	1.64×10^{-14}
14	8:19:58.6	21:07:02.2	0.7	176.47	18.09	5.29×10^{-14}
15	8:20:02.5	20:55:28.4	0.7	71.18	13.82	2.17×10^{-14}
16	8:20:18.0	21:13:35.4	0.7	68.85	13.84	2.09×10^{-14}
17	8:20:20.0	21:05:07.6	0.7	42.87	13.91	1.26×10^{-14}
18	8:20:21.9	21:08:04.3	0.7	42.78	14.07	1.25×10^{-14}
19	8:20:30.6	20:56:15.7	0.7	58.06	12.91	1.74×10^{-14}
20	8:20:33.2	21:24:47.2	1.5	113.00	25.37	3.86×10^{-14}
21	8:20:42.1	20:57:19.3	0.7	265.74	20.28	7.88×10^{-14}
22	8:20:43.4	21:08:30.8	0.7	36.06	13.38	1.06×10^{-14}
23	8:21:01.5	21:28:48.5	1.5	139.56	25.57	5.10×10^{-14}
24	8:21:02.6	20:47:31.8	1.5	451.97	32.69	1.50×10^{-13}
25	8:21:07.1	21:17:27.0	0.7	41.93	12.33	1.36×10^{-14}
26	8:21:24.7	21:27:26.0	0.7	117.98	28.14	4.36×10^{-14}
27	8:22:14.9	21:05:41.2	1.5	215.81	28.10	7.73×10^{-14}

Counts are extracted in circles of 0.′7 or 1.′5 radii (smaller for sources in denser/more confused area), and the background is estimated from an adjacent annulus. The positions are obtained from a combination of the peaks found by the detect program and "eye-judgment" of the contour map. If these sources are at the distance of NGC2563, their luminosities (1 keV spectrum with line-of-sight column densities) are in the range $\sim 10^{40} - 10^{41}$ erg s^{-1} consistent with the luminosities of normal galaxies. However, not all of the clumps are associated with galaxies, and vice versa, not all galaxies are associated with clumps in the X-ray emission. Therefore a direct association clumps-galaxies must be made with some caution. In particular, as already mentioned for the case of the Pegasus I group, inhomogeneities have been observed in other groups and clusters, apparently not associated with optical objects. The 'sources' N. 4, 6, 12 and 18 appear to coincide with early type galaxies of the Cancer subgroup A (Zw 119048, 119053, 119058, 119063 respectively), and source 27 coincides with an early type galaxy of subgroup B (Zw 119072). Source 10 is associated to a late type galaxy (Zw 119055), also from subgroup A. Most of the other clumps appear to coincide with one or more object in the "Digitized Sky Survey" plate. A detailed analysis of the spectral properties of these sources cannot be done at this stage, due to the limited statistics available.

The contour map of Fig. 9 indicates that the extended emission is probably associated only to Group A, and should be assigned a distance based on the 4705 km s^{-1} velocity that Bothun et al (1983) have estimated for that group.

(Group B is also at a much higher average velocity, v=6326 km s^{-1}). At the distance of 126.5 Mpc, $L_x \sim 1.5 \times 10^{41}$ erg s^{-1}.

The radial distribution of the emission (Fig. 3) is one of the flattest of the present sample of galaxies and is very similar to other radial distributions reported for galaxy groups (NGC 507, Kim & Fabbiano 1995;NGC 1399, Kim et al 1995). It is therefore likely that the group emission dominates also in this case outside of the inner 1' (30 kpc) *i.e.* outside of the optical size of the galaxy, as measured by the UGC (Nilson 1973). The temperature profiles also indicates that the gas is isothermal outside of the inner 1' region, where a cooler galaxy gas is found.

As shown by Table 5, to NGC2563 is associated the largest gravitational mass we have calculated. The total mass, $M_T \sim 10^{13}$ $M_\odot$, is comparable with the total masses estimated for other groups of galaxies (NGC5044, David et al 1994; NGC507, Kim & Fabbiano 1995; NGC4261, Davis et al 1995). However, our estimate is about a factor of 10 less than that derived from the dynamical properties of the group, as estimated by Bothun et al (1983). If we use our mass estimate, we can calculate the mass-to-light ratio both for the group as a whole (*i.e.* taking into account all of the optical light as given by Bothun et al.) and for the single galaxy (*i.e.* assuming that the whole X-ray emission should be attributed to NGC2563). This results in M/L in the range 10-150 respectively.

6. Other Galaxies in the Observed Groups

The present observations of the two groups (Pegasus and Cancer) are much more sensitive than those obtained with the *Einstein* instruments. The Cancer field in particular has been observed for 50000 sec., which allows us to detect sources as faint as $\geq 2 \times 10^{-14}$ erg cm^{-2} s^{-1}. This corresponds to a luminosity $L_x \sim 10^{40}$ erg s^{-1}, for the spectral parameters of Table 6 at the assumed Cancer distance. In the NGC533 field, NGC521, a bright late type galaxy in the same group (GH14, Geller & Huchra 1983) is also detected with $f_x \sim 1.4 \times 10^{-13}$ erg cm^{-2} s^{-1}, corresponding to $L_x \sim 2 \times 10^{41}$ erg s^{-1} (for a 5 keV thermal bremsstrahlung spectrum, with line-of-sight absorption). As already noticed, besides the targets, 6 of the galaxies in Cancer (5 early and one late types) and one (early type) in Pegasus have been individually detected, at fluxes $f_x \geq 2 \times 10^{-14}$ erg cm^{-2} s^{-1}. This corresponds to X-ray luminosities in the range $1\text{-}10 \times 10^{40}$ erg s^{-1}, entirely consistent with the X-ray luminosities of normal galaxies (Fabbiano et al 1992). Moreover, these are among the optically brighter objects. Therefore, given the observed trend that brighter galaxies are also on average more X-ray luminous, the lack of detection of all galaxies is entirely consistent with this trend and with the related scatter.

If the association of the excess counts with the corresponding optical galaxy is real, the X-ray to optical ratio for these objects spans from a value of ~ 29.6 for NGC2562 (source 18 in Cancer) to ~ 31 for source 27 in Cancer, associated with a Group B galaxy (ZW119072), *e.g.*, they cover the entire range observed for early type galaxies (Kim et al. 1992).

7. Conclusions

ROSAT PSPC observations of 5 X-ray bright early-type galaxies are analyzed and the spectral characteristics of the X-ray emitting hot gas that dominates the emission are derived.

The morphology of the gas appears in most cases to deviate from azimuthal symmetry, indicating that the assumption of spherical symmetry is often an oversimplification of the real distribution of the gas. Several clumps or additional sources are also observed, some of which could be related to the presence of a group emission. In the NGC2563 field several of this seemingly unrelated sources appear to coincide with galaxies in the group. Whether these are detections of individual galaxies or whether they are substructures of the group gas that coincide with the presence of a galaxy is not known. However, if these are individual galaxies, their X-ray luminosity is consistent with those of normal galaxies of the same optical luminosity (cf. Fabbiano et al 1992).

We find that the gas has an average temperature of 0.8-1 keV, and that a positive temperature gradient is suggested in a few cases. However care must be taken when comparing temperatures for different systems, since they have been sampled over very different physical regions. In NGC4649, a bright galaxy in the Virgo cluster, the gas temperatures are estimated within a 35 kpc radius, and therefore we are most certainly in the galaxy itself. In NGC2563, at the center of group A in the Cancer cluster, the observed X-ray emission extends out to ~ 400 kpc and is probably due to the whole group, while the galaxy gas only contributes (and possibly dominates) in the inner 1' region (corresponding

gradients are present only in the gas of the galaxy proper (as is the case for example of NGC 4636; Trinchieri et al 1994), then a fair comparison between objects calls for spatially resolved spectra over the same linear size, which is only achievable at the present time for a handful of the most nearby, brightest objects. Until instruments with the appropriate spatial resolution coupled with high sensitivity and spectral capability become available (such as AXAF) we are not likely to resolve the issue of what are the properties of the emission from gas dominated early type galaxies compared to those of more complex systems (groups and clusters).

The determination of temperatures and densities at different radii could in principle be used to estimate the total mass of the system. However, at large radii, where a mass measure would be most interesting, temperatures are not well determined, and often only lower limits could be derived. Estimates of the total mass therefore remain highly uncertain. Formal values are in the range of a few $\times 10^{12}$ $M_\odot$ for individual galaxies to a few $\times 10^{13}$ $M_\odot$ for groups. This leads to M/L values of $\sim$ 30-100 and to a "visible" to total mass fraction of the order of $\sim$ 20% for all systems. The Cancer group seems to be an exception, with a "visible" mass that could be as high as $\sim$ 100% of the total. However, as already discussed, the X-ray derived M_T is significantly smaller than that derived from dynamical considerations (Bothun et al 1983). The X-ray derived mass is in good agreement with similar results for other poor groups of similar dynamical properties (*i.e.* similar velocity dispersion). Since we are not aware of a systematic comparison between total mass derived from X-ray or dynamical methods for poor groups, this discrepancy could be also found in other systems.

Acknowledgements. We thank G. Gavazzi and A. Wolter for many valuable discussions. This work was supported by the Italian Space Agency and by NASA grants NAG5-2049, NAS8-39073, NAGW2681, and by the KOSEF international program.

References

Bauer, F. & Bregman, J.N. 1996, ApJ, in press
Boehringer, H, Briel, U.G., Schwarz, A., Voges, W., Hartner, G. & Truemper, J 1994, Nature, 368, 828
Bothun, G., Geller, M., Beers, T., Huchra, J., 1983 ApJ, 268, 47
Buote, D.A. & Canizares, C.R.C. 1994 ApJ 472, 86
Canizares, C.R.C., Donahue, M., Trinchieri, G., Stewart, G., and McGlynn, T. 1986 ApJ 304, 312
Chapman, G.N., Geller, M.J. and Huchra, J.P. 1988 AJ 95, 999.
David, L.P., Jones, C., Forman, W., and Daines, S. 1994 ApJ 428, 544
Davis, D., Mushotzky, R.F., Mulchaey, J.S., Worral, D.M., Birkinshaw, M., Burstein, D. 1995, ApJ 444, 528
Fabbiano, G. Kim, D-W. and Trinchieri, G. 1994 ApJ 429, 94
Fabbiano, G., Kim, D-W., and Trinchieri, G. 1992, ApJS 80, 645
Fabricant, D., Gorenstein, P 1983, ApJ 267, 535.
Forman, W., Schwarz, J. Jones, C., Liller, W., & Fabian, A.C. 1979, ApJL 234, L27.
Geller, M, Huchra, J, 1983, ApJS 52, 61
Hasinger, G. Burg, R., Giacconi, R., et al 1993, AA 275, 1
Kim D-W., Fabbiano G., & Trinchieri G. 1992 ApJ 393, 134.
Kim D.-W. & Fabbiano, G. 1995 ApJ 441, 182.
Kim D-W., et al, 1995, preprint
Kriss, G.A., Cioffi, D.F. & Canizares, C.R. 1983, ApJ 272, 439.
Nilson, P., 1973, "Uppsala General Catalogue of Galaxies", Uppsala Obs.Ann., Vol 6
Pfeffermann, E. at al 1987, Proc. SPIE 733, 519.
Prestwich, A.H., Guimond, S.J., Luginbuhl, C.B., and Joy, M. 1995, ApJ 438, L71
Price, R. Burns, J.O., Duric, N., Newberry, M.V. 1991 AJ 102, 14
Stark, A.A, Gammie, C.F., Wilson, R.W., Bally, J., Linke, R.A., Heiles, C., Hurwitz, M. 1992, ApJS 79, 77
Trinchieri, G., Fabbiano, G., & Canizares, C.R.C. 1986, ApJ, 310, 637
Trinchieri, G., Kim, D-W., Fabbiano, G., & Canizares, C.R.C. 1994, ApJ 428, 555
Truemper, J. 1983. Adv. Space Res. 2, No. 4, 241.

This article was processed by the author using Springer-Verlag LaTeX A&A style file *L-AA* version 3.